De Novo Missense Variants in *FBXW11* Cause Diverse Developmental Phenotypes Including Brain, Eye, and Digit Anomalies

Richard J. Holt,[1,26] Rodrigo M. Young,[2,3,26] Berta Crespo,[4,26] Fabiola Ceroni,[1,26] Cynthia J. Curry,[5] Emanuele Bellacchio,[6] Dorine A. Bax,[1] Andrea Ciolfi,[6] Marleen Simon,[7] Christina R. Fagerberg,[8] Ellen van Binsbergen,[7] Alessandro De Luca,[9] Luigi Memo,[10] William B. Dobyns,[11,12] Alaa Afif Mohammed,[13,14] Samuel J.H. Clokie,[13] Celia Zazo Seco,[15] Yong-Hui Jiang,[16] Kristina P. Sørensen,[8] Helle Andersen,[17] Jennifer Sullivan,[18] Zöe Powis,[19] Anna Chassevent,[20] Constance Smith-Hicks,[20] Slavé Petrovski,[21,22] Thalia Antoniadi,[13] Vandana Shashi,[18] Bruce D. Gelb,[23] Stephen W. Wilson,[2] Dianne Gerrelli,[4] Marco Tartaglia,[6] Nicolas Chassaing,[15,24] Patrick Calvas,[15,24] and Nicola K. Ragge[1,25,*]

The identification of genetic variants implicated in human developmental disorders has been revolutionized by second-generation sequencing combined with international pooling of cases. Here, we describe seven individuals who have diverse yet overlapping developmental anomalies, and who all have *de novo* missense *FBXW11* variants identified by whole exome or whole genome sequencing and not reported in the gnomAD database. Their phenotypes include striking neurodevelopmental, digital, jaw, and eye anomalies, and in one individual, features resembling Noonan syndrome, a condition caused by dysregulated RAS signaling. *FBXW11* encodes an F-box protein, part of the Skp1-cullin-F-box (SCF) ubiquitin ligase complex, involved in ubiquitination and proteasomal degradation and thus fundamental to many protein regulatory processes. FBXW11 targets include β-catenin and GLI transcription factors, key mediators of Wnt and Hh signaling, respectively, critical to digital, neurological, and eye development. Structural analyses indicate affected residues cluster at the surface of the loops of the substrate-binding domain of FBXW11, and the variants are predicted to destabilize the protein and/or its interactions. *In situ* hybridization studies on human and zebrafish embryonic tissues demonstrate *FBXW11* is expressed in the developing eye, brain, mandibular processes, and limb buds or pectoral fins. Knockdown of the zebrafish *FBXW11* orthologs *fbxw11a* and *fbxw11b* resulted in embryos with smaller, misshapen, and underdeveloped eyes and abnormal jaw and pectoral fin development. Our findings support the role of *FBXW11* in multiple developmental processes, including those involving the brain, eye, digits, and jaw.

Whole exome or whole genome sequencing (WES and WGS, respectively) has dramatically advanced the identification of genetic variants contributing to complex, rare, and clinically heterogeneous human disorders. However, because such variants might be private, it can be challenging to ascribe pathogenicity. Recently, WES and WGS and the international collation of affected individuals with variants in the same gene[1,2] have led to the identification of several developmental disorders. This approach, referred to as "reverse phenotyping," has been successfully applied to multiple intellectual disability syndromes, including those related to genetic variants in *FBXO11* (MIM: 607871),[3–5] and syndromes involving variants in *CDC42* (MIM: 116952) and *RAC1* (MIM: 602048),[6,7] all of which display clinical heterogeneity. Here, we use a similar approach to investigate the role of *de novo* variants in *FBXW11* (MIM: 605651) in human development.

[1]Faculty of Health and Life Sciences, Oxford Brookes University, Oxford OX3 0BP, UK; [2]Department of Cell and Developmental Biology, Biosciences, University College London, Gower St, London WC1E 6BT, UK; [3]Institute of Ophthalmology, University College London, 11-34 Bath Street, London EC1V 9EL, UK; [4]Great Ormond Street Institute of Child Health, University College London, London WC1N 1EH, UK; [5]Genetic Medicine, University of California, San Francisco/Fresno, Fresno, CA 93701, USA; [6]Genetics and Rare Diseases Research Division, Ospedale Pediatrico Bambino Gesù, Scientific Institute for Research, Hospitalization, and Healthcare, 00146 Rome, Italy; [7]Department of Genetics, University Medical Center Utrecht, 3508 GA Utrecht, the Netherlands; [8]Department of Clinical Genetics, Odense University Hospital, 5000 Odense C, Denmark; [9]Molecular Genetics Unit, Fondazione Casa Sollievo della Sofferenza, 71013 San Giovanni Rotondo, Italy; [10]Unità Operativa Complessa di Pediatria e Patologia Neonatale, Ospedale San Martino, 32100 Belluno, Italy; [11]University of Washington, Seattle, WA 98195-6320, USA; [12]Center for Integrative Brain Research, Seattle Children's Research Institute, Seattle WA 98101, USA; [13]West Midlands Regional Genetics Laboratory, Birmingham Women's and Children's National Health Service Foundation Trust, Mindelsohn Way, Edgbaston, Birmingham B15 2TG, UK; [14]Clinical and Chemical Pathology Department, Faculty of Medicine, Cairo University, 11562 Cairo, Egypt; [15]UDEAR, Université de Toulouse, UMRS 1056 Institut National de la Santé et de la Recherche Médicale-Université Paul Sabatier, 31059 Toulouse, France; [16]Department of Pediatrics and Neurobiology, Program in Genetics and Genomics, Duke University School of Medicine, Durham, NC 27710, USA; [17]Hans Christian Andersen Children's Hospital, Odense University Hospital, 5000 Odense C, Odense, Denmark; [18]Department of Pediatrics, Division of Medical Genetics, Duke University Medical Center, Durham, NC 27710, USA; [19]Department of Clinical Affairs, Ambry Genetics, Aliso Viejo, CA 92656, USA; [20]Department of Neurology, Division of Neurogenetics Kennedy Krieger Institute, Baltimore, MD 21205, USA; [21]Centre for Genomics Research, Discovery Sciences, Biopharmaceuticals R&D, AstraZeneca, Cambridge, CB4 0WG, UK; [22]Department of Medicine, the University of Melbourne, Melbourne, VIC 3010, Australia; [23]Mindich Child Health and Development Institute, Department of Pediatrics, and Department of Genetics and Genomic Sciences, Icahn School of Medicine at Mount Sinai, New York, NY 10029, USA; [24]Department of Medical Genetics, Purpan University Hospital, 31059 Toulouse, France; [25]West Midlands Regional Clinical Genetics Service and Birmingham Health Partners, Birmingham Women's and Children's National Health Service Foundation Trust, Birmingham, B15 2TG, UK
[26]These authors contributed equally to this work
*Correspondence: nragge@brookes.ac.uk
https://doi.org/10.1016/j.ajhg.2019.07.005.

Figure 1. Phenotypes of Individuals 1, 2, 4, 5, and 7

(A–C) Individual 1 at age 13 years, showing bilateral ptosis related to the underlying ocular anomalies (A), contractures affecting the distal interphalangeal joints of the left 4th and 5th fingers (B), and a wide sandal gap, short terminal phalanges, contractures affecting the 4th and 5th toes, 2–3 toe syndactyly, and scarring from surgery removing the left supernumerary toe (C).

(D–I) Individual 1 at age 24 years, showing bilateral microanterior segment and iris colobomas (D–G), contractures of the 4th and 5th left fingers (H), scarring from surgery removing the supernumerary toe, 2–3 toe syndactyly, and contractures of the 4th and 5th toes (I).

(legend continued on next page)

Through WES of 32 individuals with developmental eye anomalies, we identified a *de novo* missense variant (GenBank: NM_012300.2:c.1087C>T; NP_036432:p.Arg363Trp) in *FBXW11*. This variant was present in a girl with striking eye anomalies (bilateral microanterior segments, iris and chorioretinal coloboma, and lens anomalies), digital anomalies, and a psychiatric disorder (individual 1) (Figure 1, Tables 1 and S1, and the Supplemental Note). No other pathogenic variants were present in known eye development genes. Koolen et al.[8] previously described a boy with holoprosencephaly (HPE), seizures, small stature, preaxial polydactyly affecting the hand, "finger-like thumbs," and an increased sandal gap who had a *de novo* duplication encompassing seven genes, including *FBXW11,* on chromosome 5q35.1 (1.24 Mb). They hypothesized that his phenotype could be explained by the duplication of *FBXW11*, given its putative role in hedgehog (Hh) signaling and the phenotypic overlap with other disorders (HPE and polydactyly) caused by dysregulation of this pathway. Furthermore, duplication of the homologous gene *BTRC* (MIM: 603482) is implicated in split hand-foot malformation.[9] Moreover, FBXW11 participates in the Wnt/β-catenin signaling pathway,[10,11] which is fundamentally important in eye and brain development[12,13] and digit patterning.[14]

Through GeneMatcher,[2] we identified six other individuals with *de novo* missense variants in *FBXW11*; all were predicted to be damaging and found by WES or WGS. Five individuals (individuals 2–6) exhibited neurodevelopmental and/or digit anomalies, and one (individual 7) had a complex phenotype including brain anomalies and features suggestive of Noonan syndrome (Tables 1 and S1, Figure 1, and the Supplemental Note). Individual 7 had no pathogenic variants in genes currently included in Noonan syndrome or related RASopathy diagnostic panels. All genetic testing was performed under research ethics approval from the UK "Genetics of Eye and Brain anomalies" study (REC 04/Q0104/129), French (CPP Sud-Ouest and Outre-Mer II), American (Duke University, Pro00032301 - Genomic Study of Medical, Developmental, or Congenital Problems of Unknown Etiology), and Italian (Ospedale Pediatrico Bambino Gesù study 1702_OPBG_2018) ethics committees or by clinical diagnostic consent (Supplemental Material and Methods).

Our seven individuals presented with a range of overlapping phenotypes. Neurodevelopmental features commonly included neurodevelopmental delay (6/7), speech delay (5/7), autistic and/or stereotypical behaviors (3/7), psychiatric features (4/7), and micro- (1/7) or macrocephaly (3/7). MRI data from five individuals indicated corpus callosal hypoplasia (2/5), dilated ventricles (2/5), and white matter atrophy (2/5). Five of seven individuals had an under- or overdeveloped jaw. Digital anomalies were striking and included brachydactyly or short distal phalanges (3/7), polysyndactyly (2/7), widened interdigital spaces and/or sandal gap (2/7), camptodactyly or contractures (2/7), and underdeveloped thenar musculature (2/7). Individual 7 was clinically diagnosed with Noonan syndrome, and pulmonary stenosis, a recurrent feature of this disorder, was present in individual 5. Only individual 1 had developmental eye anomalies. Certain of these phenotypes overlap with those of the boy, presented by Koolen et al.,[8] who exhibited multiple digital anomalies, neurodevelopmental delay, and absence of the anterior part of the corpus callosum. From the published images, it also appears that he has broad halluces and short terminal phalanges. The latter are interesting because individual 4 had bilateral shortening of the thumbs and big toes, individuals 2, 4, and 7 had short terminal phalanges and/or brachydactyly, and individuals 2 and 4 had underdevelopment of the thenar eminence, akin to "finger-like thumbs." Although overlapping features can be seen, there is phenotypic diversity, which appears to be an emerging pattern for variants affecting genes controlling multiple cellular pathways and developmental processes; these gene include, for example, *CDC42*,[6] *FBXO11*,[3–5] *SHH* (MIM: 600725),[15,16] and *SOX2* (MIM: 184429).[17,18]

FBXW11 belongs to a highly conserved group of around 60 proteins characterized by a motif of ~40 amino acids (the F-box). This family is subdivided into three classes: FBXWs containing WD40 repeats, FBXLs containing leucine-rich repeats, and FBXOs containing either different protein-protein interaction modules or no recognizable motifs.[19] WD40-repeats are also a motif of approximately

(J–O) Individual 2 at age 9 years, showing a prominent nasal tip, broad columella, and retrognathia (J–K), the feet showing contractures (see the detailed view of the left 2nd toe), short distal digits, widely spaced toes, left 2–3 toe syndactyly, right 2nd toe clinodactyly (L and M) comparable to that of Individual 1, and MRI scans revealing an abnormal corpus callosum, an absent splenium, thick Probst bundles, small globular dysplastic hippocampi, and mildly reduced white matter volume (N and O).
(P–W) Individual 4 at age 18 years, showing dysmorphic facial features including mild ptosis of the upper eyelids, malar hypoplasia, a long and smooth philtrum, a bifid nasal tip, a thin upper lip (P), micrognathia, a tall sloping forehead, and small ears (Q); digital anomalies include shortening of the distal phalanx of the thumbs, 5th finger clinodactyly (R–U), thenar hypoplasia on the right (S), and mild thenar hypoplasia on the left (U); digital anomalies of the feet include shortening of the distal phalanx of the toes and increased convexity of all toenails (V and W).
(X–AB) Individual 5 at 4 months, showing a small chin (X), adducted thumbs not well shown as they are held by the clinician (Y and Z), and normal feet (AA and AB).
(AC) Individual 7 at 3 years and 2 months, showing frontal bossing; a deep, broad nasal bridge, epicanthus; low-set, posteriorly rotated ears; and a large, protruding tongue.
(AD–AJ) Individual 7 at 9 years and 8 months, showing frontal bossing; a deep, broad nasal bridge; epicanthus; low-set, posteriorly rotated ears (AD and AE); mild prognathism (AE); pectus carinatum (AF); and bilateral clinodactyly of the 4th and 5th toes (AG and AH). Brain MRI of Individual 7 showed complete agenesis of the corpus callosum with only a small residual portion of the anterior genum, a retro-cerebellar arachnoidal cyst (AI), and colpocephaly characterized by dilated lateral ventricles, specifically in the occipital and temporal horns and the third ventricle (AJ).

Table 1. Summary of Phenotypic and Genotypic Data of Individuals with *FBXW11* Missense Variants

Individual		1	2	3	4	5	6	7	Koolen et al. 2006[8]
Variant (GenBank: NM_012300.2; NP_036432.2)		c.1087C>T (p.Arg363Trp)	c.1091C>A (p.Ala364Asp)	c.1093G>A (p.Ala365Thr)	c.1330G>A (p.Glu444Lys)	c.1340G>A (p.Arg447Gln)	c.1340G>T (p.Arg447Leu)	c.724G>C (p.Gly242Arg)	1.24Mb duplication
gnomAD[26] frequency		absent	absent	absent	absent	absent	absent	absent	N/A
Inheritance		*de novo*	*de novo*	*de novo*	*de novo*	*de novo*	*de novo*	*de novo*	*de novo*
InterVar[77] classification		likely pathogenic	likely pathogenic	likely pathogenic	likely pathogenic	likely pathogenic	likely pathogenic	likely pathogenic	N/A
SIFT[78] classification		damaging	tolerated	damaging	damaging	damaging	tolerated	damaging	N/A
PolyPhen-2[79] classification		probably damaging	probably damaging	probably damaging	possibly damaging	probably damaging	probably damaging	probably damaging	N/A
Sex		female	male	male	female	female	male	male	male
Birth parameters	Term (weeks [+days])	40 (+5)	40	40 (+2)	39	40 (+6)	38	38	N/A
	Weight (kg)	4.08	3.63	3.95	3.15	3.17	3.40	3.22	N/A
Growth parameters (age)	Current age (years)	24	9	27	18	1	8	9 years, 7 months	19
	Weight in kg (%ile)	54 (34^{th} %)	33.2 (79^{th} %)	75 (68^{th} %)	37.5 (0.1^{st} %; −3.7 SD)	6.2 (0.1^{st} %; −3.5 SD)	30.2 (82^{nd} %)	24.5 (8^{th} %)	N/A
	Height in cm (%ile)	169 (81^{st} %)	138.4 (81^{st} %)	180 (68^{th} %)	146.2 (0.5^{th} %; −2.5 SD)	66 (2^{nd} %; −2.1 SD)	134.5 (86^{th} %)	123.5 (2^{nd} %; −2.1 SD)	157 (5.5^{th} %) (at 15 years)
	Head circumference in cm (%ile)	58.4 (>99^{th} %; +3.7 SD)	53 (64^{th} %)	55.5 (61^{st} %)	48.5 (<1^{st} %; −5.5 SD)[a]	N/A	57 (>99^{th} %; +3.5 SD)	56 (99^{th} %)	57 (92^{nd} %) (at 15 years)

(*Continued on next page*)

Table 1. ***Continued***

Individual		1	2	3	4	5	6	7	Koolen et al. 2006[8]
Congenital anomalies	Facial	yes	yes	no	yes	yes	yes	yes	yes
	Mandibular	retrognathia	retrognathia	no	micrognathia	retrognathia	no	mild prognathism	no
	Ocular	bilateral microanterior segment, lens anomalies and colobomas, R microphthalmia	severe strabismus	mild myopia	no	alternating exotropia	no	mild myopia	no
	Hand	contractures of the 4th and 5th fingers	thinning of R and L thenar musculature, short 5th metacarpal, R transverse palmar crease, and relative brachydactyly	no	thinning of thenar musculature R > L and short distal phalanges of thumbs, bilateral mild 5th finger clinodactyly	no[b]	no	brachydactyly, small hands	right preaxial polydactyly, finger-like thumbs
	Foot	L middle toe polydactyly, wide sandal gaps, 2–3 toe syndactyly, contractures of the L 4th and 5th toes	mild 2–3 toe syndactyly, 2nd toe clinodactyly, brachydactyly, wide toe spacing, contractures of the 2nd and 4th toes, short 5th metatarsal	no	short terminal phalanges, wide sandal gaps	no	no	bilateral clinodactyly of the 4th and 5th toes, brachydactyly, small feet	wide sandal gaps
	Cardiac	no	no	no	no	pulmonary stenosis	no	patent foramen ovale	ventricular septal defect
	renal or urological	no	no	no	no	R renal hypoplasia	no	no	VUR
	Skeletal	no	no	no	yes	no	no	yes	no
Development	Motor delay	no	moderate	moderate	severe	severe	mild to moderate	severe	yes
	Intellectual deficiency	no	moderate to severe	severe	severe	delayed milestones	moderate to severe	moderate to severe	mild
	Speech and language delay	no	severe	severe	severe	N/A	moderate	moderate	N/A
Behavior	ASD or psychiatric features	psychiatric issues	repetitive behaviors	classic autism	hand stereotypy, self-injurious, impulsive and aggressive behavior	N/A	ASD, anxiety	self-injurious, impulsive and aggressive behavior	N/A

(*Continued on next page*)

Table 1. ***Continued***

Individual		1	2	3	4	5	6	7	Koolen et al. 2006[8]
Neurological features	Tone	normal	increased	increased	narrow based gait	cerebral palsy	low	low	increased
	Seizures or EEG activity	N/A	mild slowing of cerebral activity	normal	N/A	N/A	N/A	normal	infrequent seizures
	MRI	N/A	hypoplasia of the corpus callosum, reduced white matter, abnormal hippocampi	N/A	normal	generalized white matter atrophy, periventricular white matter changes with ischemic damage	mild prominence of lateral ventricles	hypoplasia of the corpus callosum, mild prominence of lateral ventricles	lobar HPE, hypoplasia of the corpus callosum
Other relevant findings		none	umbilical and inguinal hernias	none	hyperkinetic	circulatory collapse at few days of age	dermal melanosis, cupped ears	webbed neck, bilateral cryptorchidism	N/A

Details of the previously reported individual with the 1.24Mb duplication[8] are included in a separate column for reference. Detailed information is provided in the Supplemental Note and Table S1. The protein domains are reported according to UniProt annotations. All variants are absent from gnomAD. Variant locations are given according to GenBank: NM_012300.2 and NP_036432.2. Clinical interpretation of genetic variants according to ACMG/AMP 2015 guidelines was automatically predicted by InterVar for missense variants. Where available, information regarding inheritance was included in the InterVar prediction. Abbreviations are as follows: ASD = autism spectrum disorder; L = left; N/A = not available; R = right; and VUR = vesicoureteric reflux.
[a]Extreme microcephaly.
[b]Adducted thumbs.

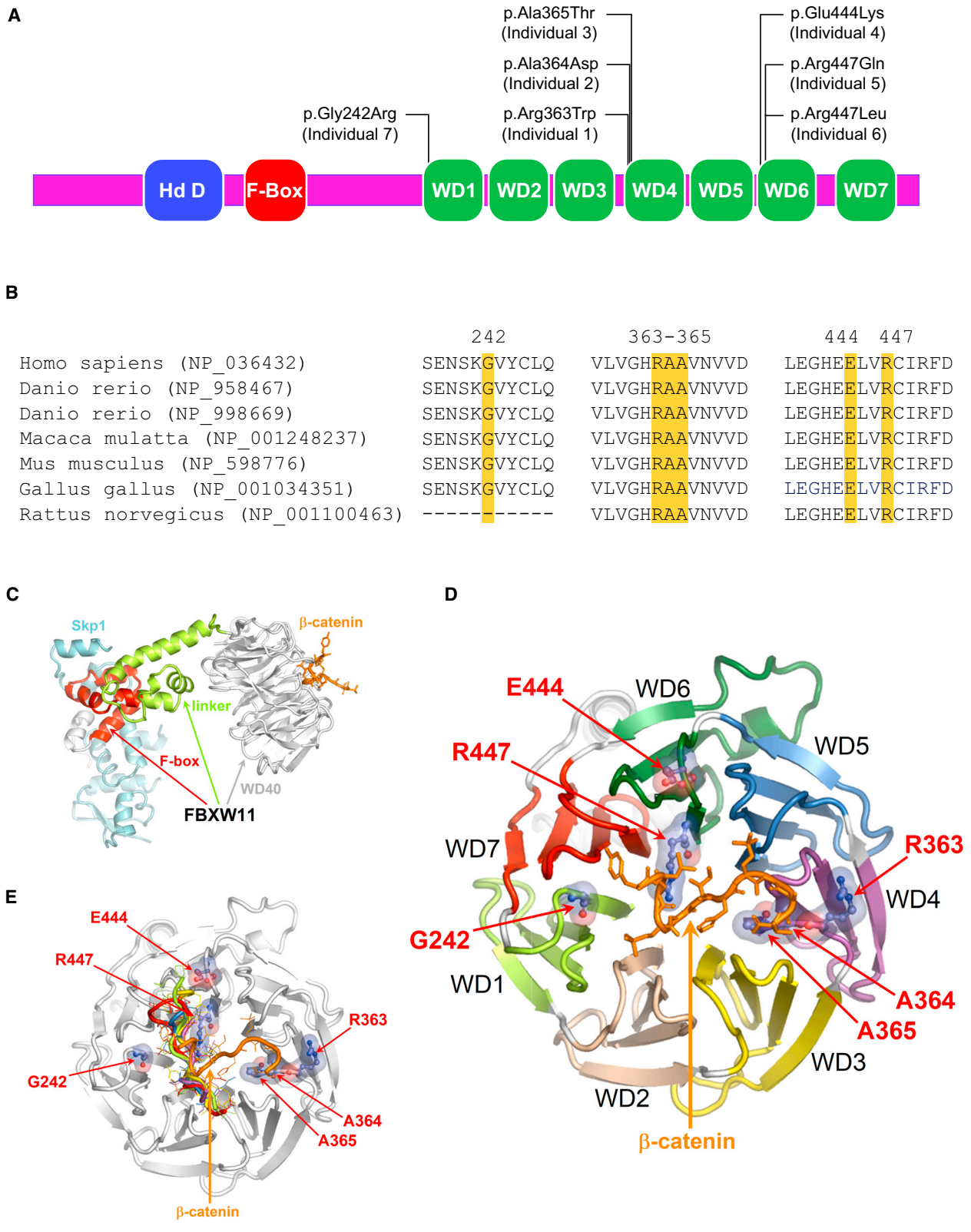

Figure 2. Structural Modeling of *FBXW11* Missense Variants
(A) A schematic representation of FBXW11 showing the relative locations of the homodimerization domain D (Hd D, blue), F-box (red), WD40 domains (green), and the missense variants identified in our seven individuals.
(B) A Clustal Omega alignment of the FBXW11 regions containing the variants identified in this study showing affected amino acids highlighted in yellow and complete conservation across species.
(C) A homology model of FBXW11 in complex with Skp1 and β-catenin based on PDB structure PDB: 1P22. Skp1 is shown in blue, β-catenin in orange, and the FBXW11 domains in red (F-box), green (linker region), and gray (WD40 domains).

(legend continued on next page)

Table 2. FoldX Predictions of the Impact on FBXW11 and BTRC Stability and Their Interactions with Skp1 and β-catenin of the *FBXW11* Variants Identified in Individuals 1–7

Individual			1	2	3	4	5	6	7
Variant			p.Arg363Trp	p.Ala364Asp	p.Ala365Thr	p.Glu444Lys	p.Arg447Gln	p.Arg447Leu	p.Gly242Arg
FBXW11	FBXW11	ΔΔG	0.521609	4.09086	4.12764	−0.0159721	1.63651	0.1246	12.0844
		Stability	minor decrease	decrease	decrease	none	decrease	none	decrease
	+ Skp1	ΔΔG	0.0	0.0	0.482	0.0	0.0	0.9022	9.6142
		Stability	none	none	minor decrease	none	none	minor decrease	decrease
	+ β-catenin	ΔΔG	0.12782	4.943962	3.866386	−0.37936	2.2931	1.55266	10.19112
		Stability	none	decrease	decrease	none	decrease	decrease	decrease
BTRC	BTRC	ΔΔG	0.51728	4.47495	3.59842	−0.10002	1.54555	0.0186672	10.264
		Stability	minor decrease	decrease	decrease	none	decrease	none	decrease
	+ Skp1	ΔΔG	0.0	0.0	0.6572	0.0	0.0	0.7318	8.8664
		Stability	none	none	minor decrease	none	none	minor decrease	decrease
	+ β-catenin	ΔΔG	0.14382	5.78723	3.457756	−0.33198	2.279382	1.5214	9.16596
		Stability	none	decrease	decrease	none	decrease	decrease	decrease

ΔΔG provided as kcal mol^{-1}. Values of ΔΔG greater than 0.46 kcal mol^{-1} indicate a decrease in stability, whereas decreases greater than −0.46 kcal mol^{-1} indicate an increase in stability. Mean values of ΔΔG for five replicate analyses of each variant are given.

40 amino acids and typically fold into a β-propeller structure that is involved in protein-protein interaction.[20,21] Alterations in other F-box genes, for example *FBXO11*[3–5] and *FBXL4* (MIM: 605654), have been associated with neurodevelopmental disorders.[22] FBXW11 is a substrate adaptor of the Skp1-cullin-F-box (SCF) ubiquitin ligase complex, which catalyzes phosphorylation-dependent ubiquitination.[11,23] It has several targets, including β-catenin and GLI transcription factors, key mediators of the Wnt and the Hh pathways, respectively. Despite the importance of these two pathways, little is known about the role of *FBXW11* in human development and the impact of aberrant FBXW11 function on human disease.

Different *in silico* metrics indicate that *FBXW11* is moderately intolerant to variation.[24,25] It has a Residual Variation Intolerance Score (RVIS) of −0.47, ranking it among the 23% of human protein-coding genes most intolerant to functional (missense, nonsense, and splice) variants.[24] Moreover, metrics reported on gnomAD (v2.1.1)[26] suggest it is intolerant to both loss-of-function (LoF) variants (observed/expected [o/e] score = 0.15, 0.08–0.31 90% confidence interval [CI]; pLI score = 0.98) and missense variants (o/e score = 0.37, 0.32–0.43 90% CI; *Z* score = 3.96). The latter is of particular relevance because all the *de novo* variants in this study are missense changes. In addition to these seven variants, two further *de novo* changes of uncertain clinical significance in *FBXW11* have been reported in large scale studies of autism spectrum disorder (ASD) (GenBank: NM_012300.2:c.243C>G [p.Asp81Glu]; dbSNP: rs995419585, c.508C>T [p.Arg170Ter]).[27,28] None of these nine variants or other changes affecting these amino acids were listed on gnomAD, with the exception of a rare synonymous variant for Ala365 (dbSNP: rs775168567, GenBank: NM_012300.2:c.1095C>T, minor allele frequency [MAF] = 0.00001771) and a missense change for Arg170 (dbSNP: rs995419585, GenBank: NM_012300.2:c.508C>G [p.Arg170Gly], MAF = 0.000003984). Furthermore, the nucleotide positions affected by our seven missense variants are evolutionarily conserved according to the GERP rejected substitutions scores[29,30] (Table S1). Interestingly, these variants are located in regions depleted for nonsynonymous variation (Figure S1). According to the model developed by Havrilla et al.,[31] six of the seven missense changes affect residues located within portions of the protein considered as under the highest constraint in the human genome, ranking among the top 5% constrained coding regions (CCRs). The amino acid substitution (c.724G>C [p.Gly242Arg]) in individual 7, who presented with features of Noonan syndrome, is located in a region characterized by a slightly lower level of constraint (85th percentile). Therefore, the location of the variants in these regions further supports their potential relevance to protein function.

Intriguingly, all seven missense variants affected the WD40 domain of FBXW11 (Figure 2). In particular, six of the seven changes appeared to cluster at the N-terminal end of the WD4 (residues 363 to 365, in individuals 1, 2, and 3, affecting consecutive amino acids) and WD6 (residues 444 and 447, in individuals 4, 5, and 6 [individuals

(D) The locations of the amino acids affected by the *FBXW11* variants within the WD40 domain. β-catenin is shown in orange.
(E) The modeled WD40 domain of FBXW11 in complex with β-catenin (orange) and other available peptides known to bind FBXW7 or Cdc4 (cyclin E C-terminal degron, cyclin E N-terminal degron, DISC1, high-affinity CPD phosphopeptide from human cyclin E, SIC1).

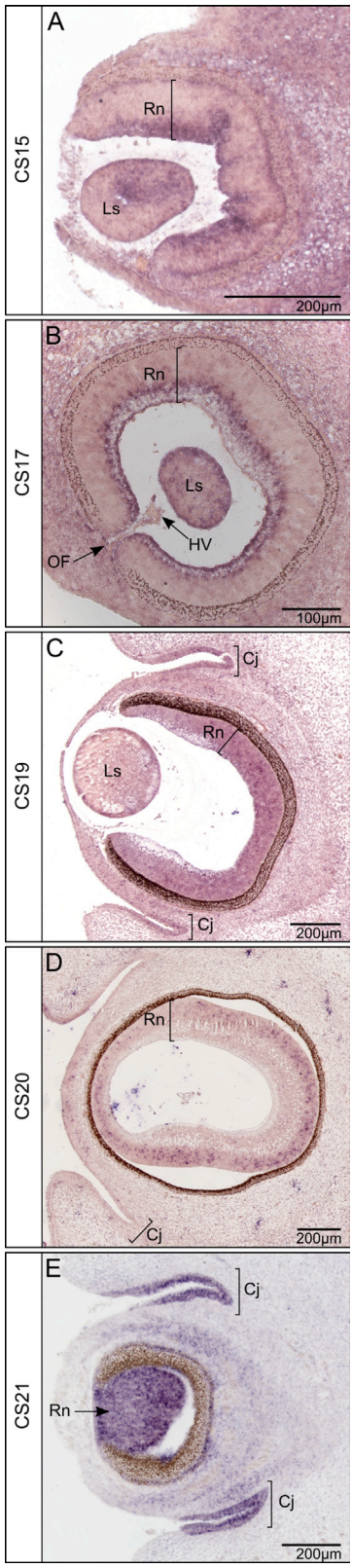

Figure 3. *In Situ* Hybridization Studies Showing *FBXW11* Expression During Human Eye Development

(A–E) Sagittal sections of the eye at CS15 (A), CS17 (B), CS19 (C), CS20 (D), and CS21 (E) made by using the 5′ UTR probe showing a strong *FBXW11* signal in the lens (A–C), the retina (A–E), the lips of the optic fissure closure (B), and regions of the developing conjunctiva (C and E). As eye development progresses, the stronger signal observed in the retina progressively shifts from the inner toward the outer retinal layers (A–D). Abbreviations are as follows: Cj = conjunctiva; HV = hyaloid vasculature; Ls = lens; OF = optic fissure; and Rn = retina.

5 and 6 had the same affected amino acid]) repeats. The seventh variant (in individual 7) affected the N-terminal end of the WD1 repeat. In contrast with this specific distribution, the two variants reported in the ASD-affected individuals[27,28] either affected a different domain of FBXW11 (p.Asp81Glu, homodimerization domain), or resulted in a truncated, likely inactive, protein (p.Arg170Ter).

No protein structure for FBXW11 was available in the Research Collaboratory for Structural Bioinformatics Protein Data Bank (RCSB PDB).[32] However, an experimentally derived crystal structure for a homolog, BTRC, complexed with Skp1 and β-catenin was available (PDB: 1P22).[20] Pairwise alignment of BTRC (GenBank: NP_003930.1) and FBXW11 (GenBank: NP_036432.2) show the proteins have 79.0% identity and 87.4% similarity, and the regions containing the missense variants in individuals 1–7 were highly conserved (Figure S2). Therefore, we modeled a 3D structure for FBXW11 (GenBank: NP_036432.2) based on the crystal structure of BTRC, employing a previously described procedure.[33] The location of the affected residues was visualized with PyMOL v2.0 (the PyMOL Molecular Graphics System, Version 2.0 Schrödinger). Notably, all affected residues were located toward the tips of the loops of the WD repeat domains, which are predicted to mediate substrate binding (Figure 2). Because there is high conservation of the WD repeat structure, and because each repeat contacts β-catenin,[20] all seven altered residues are expected to impact substrate binding. Clustering of the *de novo* missense variants suggests an impact on protein function via gain-of-function or dominant-negative mechanisms.[34] Despite this, and the fact that the phenotypes of these individuals fall in broad, overlapping categories, there is variation in the specifics of their features. We modeled the WD40 domain of FBXW11 bound to substrates of the WD40-domain-containing proteins FBXW7 and Cdc4 (Figure 2E). This indicated that individual substrates might adopt different orientations when binding to FBXW11, suggesting a variable contribution of the different WD40 motifs in FBXW11 binding to individual ligands. Therefore, it is possible that the missense variants identified here might have varying impacts depending on the substrate.

We investigated the impact of the missense variants on protein stability and interaction with Skp1 and β-catenin for both our modeled FBXW11 structure and BTRC by using FoldX.[35] Predictions indicated five of the seven missense variants (c.1087C>T [p.Arg363Trp]; c.1091C>A [p.Ala364Asp]; c.1093G>A [p.Ala365Thr]; c.1340G>A [p.Arg447Gln]; and c.724G>C [p.Gly242Arg]) impact the stability of both FBXW11 and BTRC (Table 2). Furthermore, five of the variants (p.Ala364Asp, p.Ala365Thr, p.Arg447Gln, p.Arg447Leu, and p.Gly242Arg) were predicted to decrease the stability of the FBXW11-β-catenin and BTRC-β-catenin

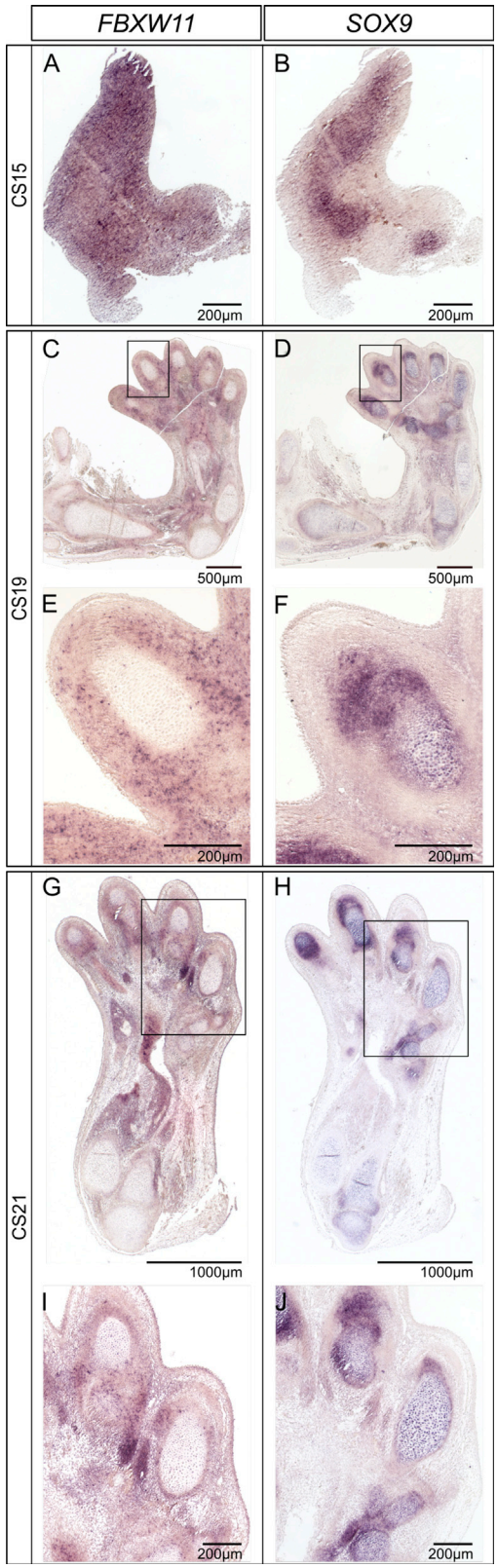

Figure 4. *In Situ* Hybridization Studies Comparing *FBXW11* and *SOX9* Expression During Human Limb Development

(A–J) Coronal sections of the forelimb at different CS stages showing the expression pattern of *FBXW11* (5′ UTR probe) on the left (A, C, E, G, and I) and the chondrogenic marker *SOX9* on the right (B, D, F, H, and J). E, F, I, and J show increased magnification of the boxed regions at CS19 (C and D) and CS21 (G and H) highlighting *FBXW11* expression around the developing cartilage of the digits in the hand plate.

interactions. Three variants (p.Ala365Thr, p.Arg447Leu, and p.Gly242Arg) also decreased the stability of the FBXW11-Skp1 and BTRC-Skp1 interactions (Table 2). Interestingly, the variant (p.Gly242Arg) in individual 7, who presented with features of Noonan syndrome, was predicted to have the greatest impact on both FBXW11 and BTRC stability and their interactions with β-catenin and Skp1. On the basis of these analyses, the variants are predicted to produce variable downstream effects and resultant phenotypes, particularly because FBXW11 is involved in multiple developmental pathways.

Next, we determined the expression profile of *FBXW11* during human development by using nonradioactive RNA *in situ* hybridization on human embryo sections from Carnegie Stages (CS) 15–21, obtained from the MRC/Wellcome Trust Human Developmental Biology Resource, UCL, with full ethical approval.[36] We designed two probes to target all three *FBXW11* human isoforms (GenBank: NM_012300, NM_033644, and NM_033645) (Supplemental Material and Methods). Both probes showed similar expression patterns (Figures 3–5 and S3–S6).

In the eye, *FBXW11* expression was seen throughout the lens at multiple time points (Figures 3A–3C, S3A–S3F, S3I, and S3J), a fact of particular relevance to the congenitally absent and thin lenses in individual 1. In the retina, *FBXW11* expression appeared to shift over time from the inner to outer neuroretinal cell layers (Figures 3A–3D). Sagittal sections of the eye at CS17 also showed *FBXW11* expression at the margins of the optic fissure (Figures 3B, S3C, and S3D), indicating a potential role in optic fissure closure, relevant to the bilateral chorioretinal colobomas in individual 1. Expression of *FBXW11* was also seen in the developing conjunctiva (Figures 3C, 3E, and S3E–S3J).

In the developing hand, expression of *FBXW11* was analyzed in parallel with expression of the chondrogenic marker *SOX9* (MIM: 608160).[37] At CS15, a strong signal was detected for both genes (Figures 4A, 4B, S4A, and S4B); *FBXW11* displayed more widespread expression throughout the limb bud compared with the restricted expression pattern of *SOX9*. At CS19 and CS21, after the digits have begun to form, strong *FBXW11* expression was seen in the mesenchyme surrounding the developing cartilage (Figures 4C–4J and S4C–S4J). Interestingly, digital anomalies were observed in four of the individuals we report, as well as the boy reported by Koolen et al.[8]

In the brain, *FBXW11* expression was present in the primitive ventricles (CS17 and CS19, Figures 5A–5C, S5A, S5B, S6A, and S6 B), metencephalon (CS19, Figures 5C, S5B, and S6B), hypothalamus (CS17, Figure 5D), and medulla (CS17, Figure 5E). These expression patterns are consistent with the altered brain structure, including prominence of the lateral ventricles and periventricular

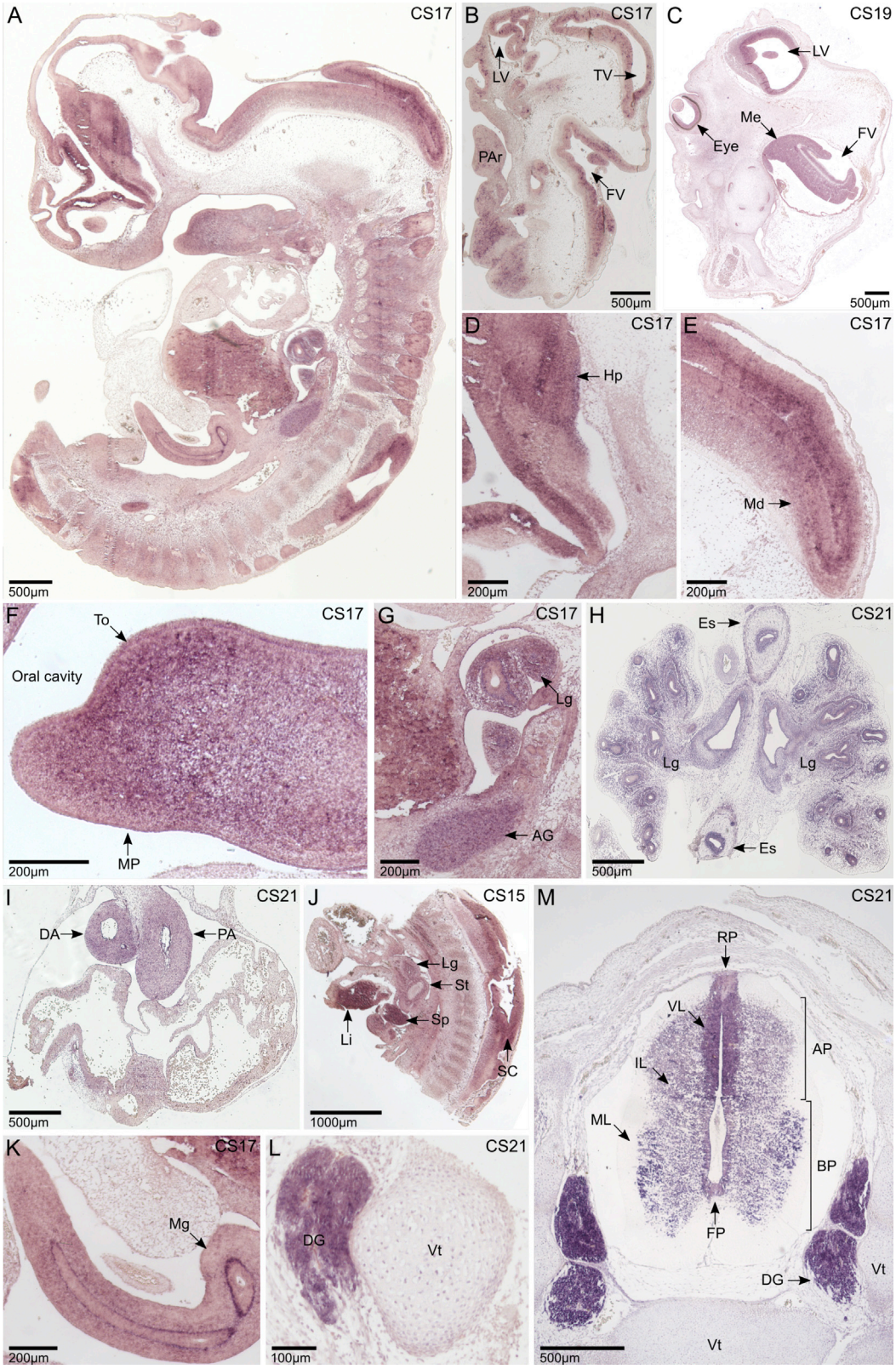

Figure 5. *In Situ* Hybridization Studies of *FBXW11* in the Human Showing the Expression Pattern in Multiple Structures during Embryonic Development

Experiments performed using the 5′ UTR probe. Structures of interest are indicated by arrows.

(A) A sagittal section of embryo at CS17 (week 6), showing *FBXW11* expression in multiple developing structures.

(B) A sagittal section of the head at CS17 (week 6) indicating expression in the structures forming the lateral, third, and fourth ventricles.

(C) A sagittal section of the head at CS19 (week 7) showing strong expression in the regions surrounding the lateral ventricle and the metencephalon.

(legend continued on next page)

changes, of individuals 2, 5, 6, and 7. Furthermore, this finding supports an important role for FBXW11 in pathways, including the Hh and the Wnt cascades, essential for normal brain development.[38,39] Strong expression was also observed in the pharyngeal arches, including the mandibular process and tongue (CS17, Figures 5F, S5C, and S6C). Expression in these structures might relate to the micrognathia or retrognathia of four of the reported individuals (1, 2, 4, and 5) and the large tongue in individual 7. Other structures showing expression included: the adrenal glands (CS17, Figures 5G, S5D, and S6D), the lungs (CS17 and CS21, Figures 5G, 5H, S5E, and S6E), the pulmonary artery and dorsal aorta (CS21, Figures 5I, S5F, and S6F), the liver (CS15, Figures 5J, S5G, and S6G), the spleen (CS15, Figures 5J, S5G, and S6G), and the midgut (CS17, Figures 5K, S5H, and S6H); the dorsal ganglia (CS21, Figures 5L, S5I, and S6I) and the spinal cord (CS15, Figures 5J, S5G, and S6G; CS17 Figures 5A, S5A, and S6A; and CS21, Figures 5M, S5J, and S6J), where the signal was detected in the floor plate, the roof plate, and the ventricular and intermediate layers of the spinal cord (CS21, Figures 5M, S5J, and S6J). The expression in the pulmonary artery and dorsal aorta is interesting given the pulmonary stenosis seen in individual 5.

The zebrafish genome includes two orthologs of *FBXW11*, *fbxw11a* and *fbxw11b*. These genes encode proteins with 90.4% sequence identity and 95.3% similarity. Furthermore, both zebrafish orthologs share around 85% identity and 91% similarity with human FBXW11 (GenBank: NP_036432.2) (Fbxw11a [GenBank: NP_958467.1]: 84.7% identity, 90.6% similarity; Fbxw11b [GenBank: NP_998669.2]: 85.6% identity, 91.2% similarity). We performed *in situ* hybridization with probes designed against the low homology 3′ UTR region of *fbxw11a* and *fbxw11b* to avoid cross-detection (Supplemental Material and Methods).[40] At 4 days post fertilization (dpf), *fbxw11a* is expressed at low levels in the retina and brain and higher levels in the jaw mesenchyme (Figure 6A). *fbxw11b* is expressed widely in the brain and eyes, and there are high levels in the retinal ganglion layer, inner nuclear layer, in or adjacent to the outer plexiform layer, in the photoreceptor layer, ciliary marginal zone, jaw mesenchyme, oral epithelia (Figure 6B), and pectoral fins (Figures S7A–S7D). These findings are comparable to the expression data in humans, further supporting a role for *FBXW11* in the development of the eye, jaw, limbs, and brain.

To further investigate the role of *FBXW11* in vertebrate development, we generated zebrafish knockdown models by using a combination of morpholino and CRISPR-Cas9 technologies (Supplemental Material and Methods). Morpholino knockdown of *fbxw11a* resulted in no overt phenotype in zebrafish embryos (Figures S7E and S7F). *fbxw11b* morphants consistently showed reduced eye size and a shorter and bent axis phenotype (Figures S7E and S7G). Because morpholinos can have off-target effects, using CRISPR-Cas9 we induced a 7bp frameshift mutation (allele u5010, p.Asp24Leufs*6) in *fbxw11b* exon 2 (Figures 6C and S7H–S7K). $fbxw11b^{u5010/u5010}$ homozygous embryos showed no abnormal phenotype and were viable and fertile. Maternal zygotic (MZ) mutant $fbxw11b^{u5010/u5010}$ embryos from an $fbxw11b^{u5010/u5010}$ female to $fbxw11b^{+/u5010}$ male cross also showed no abnormal phenotype (Figures 6D and 6E).

We hypothesized that compensation by *fbxw11a* could result in the absence of phenotype in $MZfbxw11b^{u5010/u5010}$ embryos. For instance, recent studies have shown that the loss of function of a gene resulting from nonsense-mediated decay (NMD) might be compensated for by altered expression of other genes.[41–43] Because our CRISPR-Cas9 *fbxw11b* mutant carries a frameshift mutation, it might be subject to NMD. Therefore, the lack of phenotype observed might be a result of compensatory gene expression, possibly by *fbxw11a*. However, *in situ* hybridization experiments did not show any obvious upregulation of *fbxw11a* in *fbxw11b* mutants at 48 h post fertilization (hpf) (not shown). Therefore, the basal level of expression of *fbxw11a* might be sufficient to compensate for the lack of function of *fbxw11b*. To begin to address this issue, we injected *fbxw11a* morpholino ($mo^{fbxw11a}$) in $MZfbxw11b^{u5010/u5010}$ and sibling embryos. No overt phenotype was generated before 2dpf in any genotype, and no phenotype was observed in morpholino-injected heterozygous or wild-type siblings at any stage examined. By 3dpf, $MZfbxw11b^{u5010/u5010}/mo^{fbxw11a}$ morphants showed abnormally developed pectoral fins and heart edema (Figures 6D–6I, n = 20/21); this is of interest given the digital anomalies in the individuals presented here. At 5dpf, $MZfbxw11b^{u5010/u5010}/mo^{fbxw11a}$ morphant knockdown

(D–G) Increased magnification of structures from (A) highlighting *FBXW11* expression in the hypothalamus (D), lower medulla (E), pharyngeal arches (F), and the adrenal glands and lungs (G).
(H) A coronal section at CS21 (week 8) showing expression in the lungs.
(I) A coronal section of the heart at CS21 showing *FBXW11* expression in the dorsal aorta and the pulmonary artery.
(J) A sagittal section of the embryo at CS15 (week 5) highlighting strong *FBXW11* expression in the liver, spleen, and spinal cord.
(K) Increased magnification of (A) showing *FBXW11* expression in the midgut.
(L) A transverse section at CS21 showing a strong *FBXW11* signal in the dorsal ganglia.
(M) A transverse section of the spinal cord at CS21 showing *FBXW11* expression in the floor plate, roof plate, and the ventricular and the intermediate layers of the spinal cord.
Abbreviations are as follows: AG = adrenal glands; AP = alar plate; BP = basal plate; DA = dorsal aorta; DG = dorsal ganglia; Es = Esophagus; FP = floor plate; FV = fourth ventricle; Hp = hypothalamus; IL = intermediate layer; Lg = lungs; Li = liver; LV = lateral ventricle; Md = medulla; Me = metencephalon; Mg = midgut; ML = marginal layer; MP = mandibular process; PA = pulmonary artery; Par = pharyngeal arches; RP = roof plate; SC = spinal cord; Sp = spleen; St = stomach; To = tongue; TV = third ventricle; VL = ventricular layer; and Vt = vertebra.

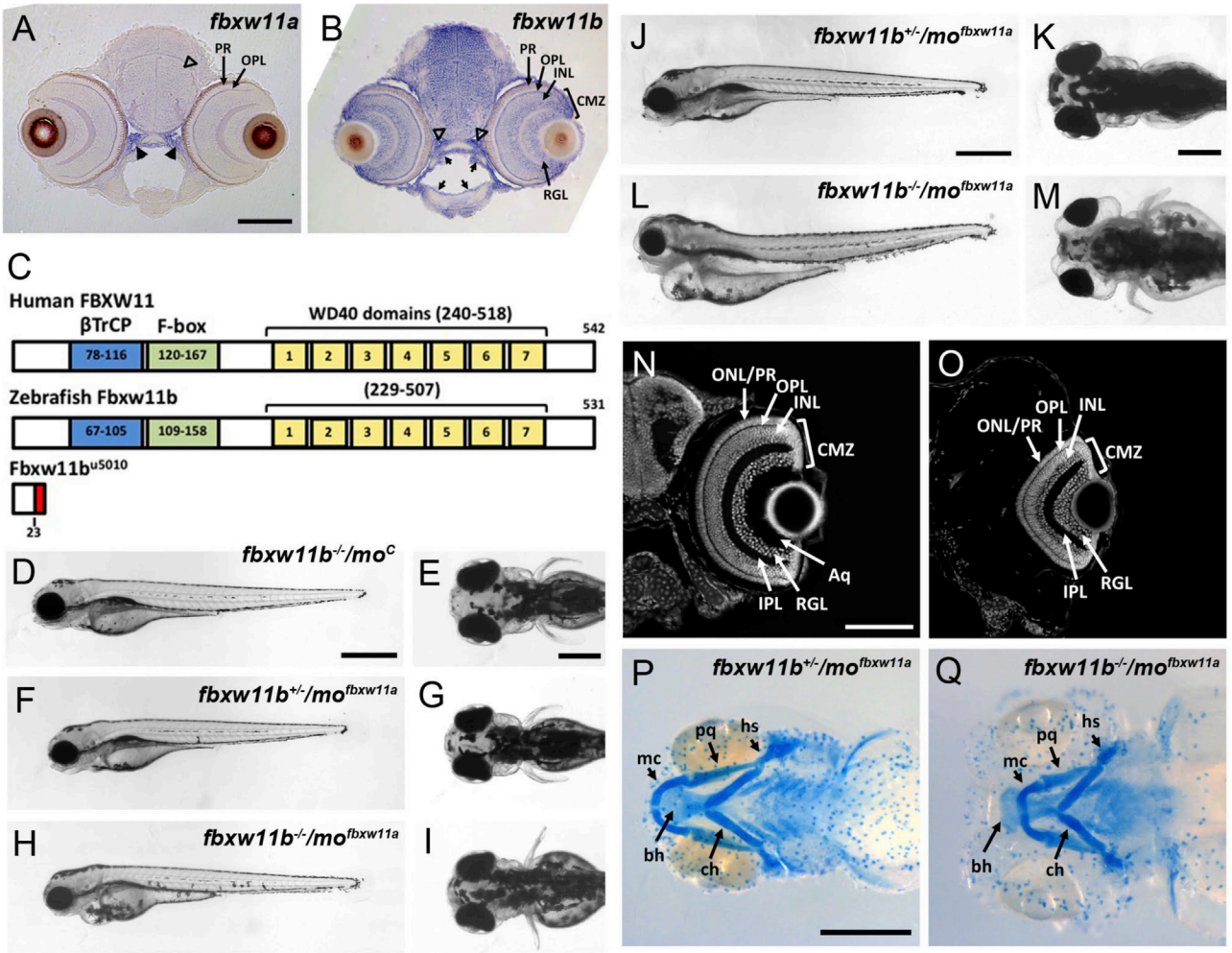

Figure 6. *fbxw11a* and *fbxw1b* Are Expressed in the Zebrafish Eye, and Their Knockdown Leads to Abnormal Eye and Jaw Development
(A and B) Coronal plastic sections showing the expression pattern of *fbxw11a* (A) and *fbxw11b* (B) in 4dpf zebrafish heads detected by *in situ* hybridization. Dorsal is up. The scale bar in (A) is 100μm.
(C) Diagram of human FBXW11 and zebrafish Fbxw11b and Fbxw11b$^{\mathbf{u5010}}$. The βTrCP domain is in blue, the F-box domain is in green, the seven WD40 domains are in yellow, and the nonsense sequence of Fbxw11b$^{\mathbf{u5010}}$ is in red. The numbers are amino acid positions in respective proteins.
(D–I) 3dpf live zebrafish *MZfbxw11*$^{\mathbf{u5010/u5010}}$ (D, E, H, and I) and *MZfbxw11b*$^{+/\mathbf{u5010}}$ (F and G) embryos injected with 500pg of control (D and E) or *fbxw11a* (F–I) morpholinos. Lateral (D, F, and H) and dorsal (E, G, and I) view, both anterior to left. The scale bar in (D) is 400μm and in (E) is 200μm.
(J–Q) 5dpf zebrafish *MZfbxw11b*$^{+/\mathbf{u5010}}$ (J, K, N, and P) and *MZfbxw11*$^{\mathbf{u5010/u5010}}$ (L, M, O, and Q) embryos injected with 500pg *fbxw11a* morpholino. (J–M) Live embryos lateral (J and L) and dorsal (K and M) view, both anterior to left. The scale bar in (J) is 400μm and in (K) is 200μm.
(N and O) Confocal imaging of DAPI-stained coronal plastic sections. The scale bar in (N) is 100μm.
(P and Q) Alcian blue staining of cartilage structures. Ventral view, anterior to left. The scale bar in (P) is 200μm.
Abbreviations are as follows: Aq = aqueous humor; bh = basihyal; ch = ceratohyal; CMZ = ciliary marginal zone; hs = hyosymplectic; INL = inner nuclear layer; IPL = inner plexiform layer; mc = Meckel's cartilage; ONL = outer nuclear layer; OPL = outer plexiform layer; pq = palatoquadrate; PR = photoreceptor layer; and RGL, retina ganglion layer.

embryos developed periocular edema and smaller eyes compared to *MZfbxw11b*$^{+/u5010}$/*mo*^{fbxw11a} knockdown heterozygous siblings (Figures 6J–6M, n = 20/20). Coronal sections showed that 5dpf *MZfbxw11b*$^{u5010/u5010}$/*mo*^{fbxw11a} knockdown eyes had all the retinal layers present in the wild-type; however, the eye was smaller and misshapen. This was potentially because of a lack of aqueous humor in *MZfbxw11b*$^{u5010/u5010}$/*mo*^{fbxw11a} knockdowns, although it was present in the phenotypically normal siblings at the same stage (Figures 6N and 6O). The reduction in eye size in mutant knockdown fish supports a role for *FBXW11* in eye development and supports the *FBXW11* variant's being implicated in the microphthalmia observed in individual 1. Alcian blue cartilage staining in *MZfbxw11b*$^{u5010/u5010}$/*mo*^{fbxw11a} knockdowns revealed abnormal development of the jaw (Figures 6P and 6Q). The basihyal (pharyngeal arch) cartilage structure protruded anteriorly in *MZfbxw11b*$^{u5010/u5010}$/*mo*^{fbxw11a} knockdowns because of shorter Meckel's and palatoquadrate cartilages (Figures 6P and 6Q). These latter observations are consistent

with four of our individuals presenting with retrognathia or micrognathia.

FBXW11 has been shown to negatively regulate the Wnt/β-catenin pathway.[44] Inhibition of Wnt/β-catenin signaling is required for the correct specification of forebrain territories, and enhanced Wnt activity leads to embryos with smaller or no eyes.[45,46] Enhanced Wnt activity in *tcf7l1a* mutants results in a smaller eye field and reduced eye size by 32hpf.[47] To determine whether Wnt/β-catenin signaling was affected in *fbxw11b*$^{u5010/u5010}$ embryos, we assessed whether there were any genetic interactions between the mutated forms of *fbxw11b* and *tcf7l1a*. As previously shown,[47] *tcf7l1a*$^{-/-}$ eyes were close to 50% of the size of wild-type eyes (Figure S8A). However, *fbxw11b* $^{u5010/u5010}$/*tcf7l1a*$^{-/-}$ double mutant embryos developed even smaller eyes, about 80% of the size of eyes in *tcf7l1a* embryos (Figure S8A, p = 0.0001, *tcf7l1a*$^{-/-}$ embryos, $\tilde{x}$ = 910.337μm^3 ± 118e^3 n = 20; *fbxw11b* $^{u5010/u5010}$/*tcf7l1a*$^{-/-}$ embryos, $\tilde{x}$ = 727.588 ± 145e,^{3} n = 19). This suggests that abrogation of *fbxw11b* leads to further enhanced Wnt signaling in *tcf7l1a*$^{-/-}$ mutants. Furthermore, exposure of embryos to a low dose of the Wnt/β-catenin agonist BIO (0.5μm treatment from 24hpf onward) led to an upward bent trunk in *fbxw11b*$^{u5010/u5010}$/*mo*^{fbxw11a} knockdown embryos but not in *fbxw11b*$^{u5010/u501}$ or wild-type embryos (Figures S8B–S8D, 100% n = 13, two experiments). This morphology is similar to that observed in APC mutants in which the Wnt pathway is constitutively overactivated.[48] Overall, these results suggest that the *fbxw11b*$^{u5010/u5010}$/*mo*^{fbxw11a} knockdown embryos are sensitized to the effects of enhanced Wnt/β-catenin activity.

Given the phenotype of individual 1 and our *in situ* and zebrafish data, we further explored whether *FBXW11* variants contribute more widely to developmental eye disorders by performing targeted screening in an additional 263 individuals with anophthalmia, microphthalmia, or coloboma (AMC) by using high-resolution melt curve analysis[49] or Sanger sequencing (Supplemental Material and Methods). Excluding three 3′ UTR private variants (c.*4064_*4065insT [chr5:171,288,698–171,288,699], c.*2867G>A [chr5:171,289,855], c.*2592C>T [chr5:171,290,168]; GenBank: NM_012300.2, GRCh37/hg19) inherited from unaffected parents, no functionally relevant variants were identified. Similarly, array comparative genome hybridization (aCGH) analysis of 77 individuals, including individual 1, with isolated or syndromic AMC did not identify any copy number aberrations affecting *FBXW11*. This indicates variants in *FBXW11* might only rarely be associated with human AMC.

FBXW11 is involved in multiple developmental pathways, including Wnt signaling, which plays a crucial role in the regulation of cell proliferation, tissue patterning, and organ morphogenesis. Wnt signaling can be divided into canonical and non-canonical pathways; and a key element of the former is ubiquitination of β-catenin (Figures S9A and S9B).[10,50] This ubiquitination, controlled by the SCF complex, is directed either by BTRC or its paralog BTRC2, encoded by *BTRC* and *FBXW11*, respectively.[11,51] Aberrations of this pathway can lead to a range of human pathologies, including developmental disorders affecting the limbs, as well as neurodevelopmental and psychiatric disorders.[10,52,53] There is also significant evidence of the importance of Wnt signaling in developmental eye disorders in mouse models.[54,55]

FBXW11 is also involved in Hh signaling by regulating the ubiquitination of GLI transcription factors (Figures S9C and S9D). Variants in Hh pathway genes are associated with developmental anomalies, some of which are comparable to those observed in the individuals presented here. Copy number gains encompassing *BTRC* are linked with developmental limb anomalies.[9,56] *Drosophila* with mutations in *Slimb,* the ortholog of both *FBXW11* and *BTRC*, develop supernumerary limbs or ectopic legs and eye anomalies.[57–59] In mice, mutations of GLI transcription factors can cause multiple malformations, including polydactyly, anophthalmia, and coloboma.[60–63] Finally, in humans, genetic variants affecting members of the Hh signaling pathway, such as *SHH* and *PTCH1* (MIM: 601309), have been associated with developmental eye anomalies and HPE.[15,64–66] *GLI2* (MIM: 165230) and *GLI3* (MIM: 165240) variants have also been reported in individuals with a variety of phenotypic features including HPE, polydactyly, and anophthalmia.[67–70] However, some of the *GLI2* variants have subsequently been classified as benign in ClinVar.

Individual 7 presented with distinctive characteristics of Noonan syndrome, a phenotype linked to RAS-MAPK signaling dysregulation.[71,72] Ras trafficking and activity are regulated by several mechanisms, including ubiquitination, which can be mediated by different ubiquitin ligase complexes.[73] Recent studies have also identified a circuit involving LZTR1, a Kelch-domain-containing protein altered in Noonan syndrome. LZRT1 functions as a substrate receptor in the cullin 3 ubiquitin ligase complex involved in the ubiquitination and functional down modulation of HRAS.[33,74,75] Interestingly, the SCF-β-TrCP E3 ligase complex has also been implicated in the ubiquitination and proteasomal degradation of HRAS,[76] supporting an unanticipated functional link between FBXW11 and RAS signaling modulation warranting further exploration.

Our structural analyses provide evidence of the specific impact of the identified variants on FBXW11 function, as well as for the dominant role of these amino acid changes. Specifically, the variants are predicted to impair proper recognition and/or binding of substrates by the SCF ubiquitin ligase complex. In contrast to the presently reported variants, the two *de novo* changes previously reported in the ASD-affected individuals are predicted to alter protein function by different mechanisms. The exon 3 missense variant is located within the homodimerization domain and might interfere with protein dimerization. Instead, the nonsense substitution affecting exon 4 is predicted to lead to NMD or a truncated protein, potentially reducing the amount of functional protein. Although several of

our individuals presented with features of ASD, little clinical information is available for the individuals from these ASD studies, except that the individual carrying the nonsense variant has a high IQ.[28] This limits our ability to suggest further how these alternate mechanisms might contribute to phenotypic variation.

In conclusion, we report seven unrelated individuals presenting with phenotypes including eye, digital, and jaw anomalies, and neurodevelopmental or psychiatric disorders. These individuals all carry *de novo* probably pathogenic missense variants in *FBXW11*, a member of the ubiquitin ligase SCF complex that functions as a regulator of both the Wnt and Hh signaling developmental pathways. *In silico* analyses provide a model for the functional impact of the variants; *in vitro* experiments with human and zebrafish developmental tissue supported early expression of *FBXW11* in relevant structures and *in vivo* zebrafish studies documented the relevance of FBXW11 in developmental processes affected in this phenotypic series. Collectively, these data support the role of *FBXW11* variants in human developmental disorders affecting the brain, eye, jaw, and digits, possibly via modulation of the Wnt/β-catenin, Hh, and RAS signaling pathways.

Supplemental Data

Supplemental Data can be found online at https://doi.org/10.1016/j.ajhg.2019.07.005.

Acknowledgments

We would like to thank the families for their participation in our study. We are grateful to the West Midlands Regional Clinical Genetics Service and, in particular, Shaun Green for their help with sample processing and clinical genetic testing of UK families with AMC conditions. Data for individual 4 were obtained by the Duke Genome Sequencing clinic supported by the Duke University Health System. We would also like to thank Rebecca Spillmann (Duke Pediatric Medical Genetics, Duke University Medical Center, Durham, NC, USA), Ioana Cutcutache, Matthew Page (Translational Medicine, UCB Pharma, Slough, UK) and Martin Armstrong (Translational Medicine, UCB Pharma, Braine-l'Alleud, Belgium).

This work was supported by grants from Baillie Gifford; Visually Impaired Children Taking Action (VICTA) (www.victa.org.uk); Microphthalmia, Anophthalmia and Coloboma Support (MACS) (www.macs.org.uk); HEIF (Health Innovation Fund, Oxford Brookes University); La Fondation de France (grant number 2015-00060235, 2015); Fondation Maladies Rares and Retina France; Fondazione Bambino Gesù (Vite Coraggiose); E-Rare (NSEuroNet); AIRC (the Italian Foundation for Cancer Research) (IG 21614); the Italian Ministry of Health (Ricerca Corrente); and the National Heart, Lung, and Blood Institute (R35 HL135742). French patients are part of the Rare Disease Cohort (RaDiCo)-AC-Oeil. RaDiCo is funded by the French National Research Agency under the specific program "Investments for the Future," cohort grant agreement ANR-10-COHO-0003. V.S. and J.S. were supported by UCB Celltech and the Duke Genome Sequencing Clinic grant. W.B.D. was supported by the US National Institutes of Health under the National Institute of Neurological Disorders and Stroke (NINDS) grant R01NS058721. R.M.Y. and S.W.W. were supported by an MRC (Medical Research Council) Programme Grant (MR/L003775/1 to S.W.W. and G. Gestri) and a Wellcome Trust Investigator Award (104682/Z/14/Z). The human embryonic and fetal material was provided by the Joint MRC/Wellcome Trust (grant MR/R006237/1) Human Developmental Biology Resource (www.hdbr.org).

Declaration of Interests

Zöe Powis was an employee of Ambry Genetics. Slavé Petrovski is Vice-president and Head of Genome Analytics for AstraZeneca Centre for Genomics Research (CGR), Cambridge, UK.

Received: March 1, 2019
Accepted: July 9, 2019
Published: August 8, 2019

Web Resources

Allen Brain Atlas, https://www.brain-map.org/
ANNOVAR, http://annovar.openbioinformatics.org/
CCR Browser, https://s3.us-east-2.amazonaws.com/ccrs/ccr.html
ClinVar, https://www.ncbi.nlm.nih.gov/clinvar/
EMBOSS Needle, https://www.ebi.ac.uk/Tools/psa/emboss_needle/
ExAC, http://exac.broadinstitute.org/
GeneMatcher, https://genematcher.org/
gnomAD, https://gnomad.broadinstitute.org/
InterVar, http://wintervar.wglab.org/
OMIM, https://www.omim.org/
Picard, http://broadinstitute.github.io/picard/index.html
POVRay, www.povray.org/
PyMOL, https://pymol.org/2/
RCSB Protein Data Bank, www.rcsb.org
UCSC Genome Browser, https://genome.ucsc.edu/
YASARA, www.yasara.org

References

1. Philippakis, A.A., Azzariti, D.R., Beltran, S., Brookes, A.J., Brownstein, C.A., Brudno, M., Brunner, H.G., Buske, O.J., Carey, K., Doll, C., et al. (2015). The Matchmaker Exchange: A platform for rare disease gene discovery. Hum. Mutat. *36*, 915–921.
2. Sobreira, N., Schiettecatte, F., Valle, D., and Hamosh, A. (2015). GeneMatcher: A matching tool for connecting investigators with an interest in the same gene. Hum. Mutat. *36*, 928–930.
3. Fritzen, D., Kuechler, A., Grimmel, M., Becker, J., Peters, S., Sturm, M., Hundertmark, H., Schmidt, A., Kreiß, M., Strom, T.M., et al. (2018). De novo FBXO11 mutations are associated with intellectual disability and behavioural anomalies. Hum. Genet. *137*, 401–411.
4. Gregor, A., Sadleir, L.G., Asadollahi, R., Azzarello-Burri, S., Battaglia, A., Ousager, L.B., Boonsawat, P., Bruel, A.L., Buchert, R., Calpena, E., et al.; University of Washington Center for Mendelian Genomics; and DDD Study (2018). De novo variants in the F-box protein FBXO11 in 20 individuals with a variable neurodevelopmental disorder. Am. J. Hum. Genet. *103*, 305–316.

5. Jansen, S., van der Werf, I.M., Innes, A.M., Afenjar, A., Agrawal, P.B., Anderson, I.J., Atwal, P.S., van Binsbergen, E., van den Boogaard, M.J., Castiglia, L., et al. (2019). De novo variants in FBXO11 cause a syndromic form of intellectual disability with behavioral problems and dysmorphisms. Eur. J. Hum. Genet. *27*, 738–746.
6. Martinelli, S., Krumbach, O.H.F., Pantaleoni, F., Coppola, S., Amin, E., Pannone, L., Nouri, K., Farina, L., Dvorsky, R., Lepri, F., et al.; University of Washington Center for Mendelian Genomics (2018). Functional dysregulation of CDC42 causes diverse developmental phenotypes. Am. J. Hum. Genet. *102*, 309–320.
7. Reijnders, M.R.F., Ansor, N.M., Kousi, M., Yue, W.W., Tan, P.L., Clarkson, K., Clayton-Smith, J., Corning, K., Jones, J.R., Lam, W.W.K., et al.; Deciphering Developmental Disorders Study (2017). RAC1 missense mutations in developmental disorders with diverse phenotypes. Am. J. Hum. Genet. *101*, 466–477.
8. Koolen, D.A., Herbergs, J., Veltman, J.A., Pfundt, R., van Bokhoven, H., Stroink, H., Sistermans, E.A., Brunner, H.G., Geurts van Kessel, A., and de Vries, B.B. (2006). Holoprosencephaly and preaxial polydactyly associated with a 1.24 Mb duplication encompassing FBXW11 at 5q35.1. J. Hum. Genet. *51*, 721–726.
9. Li, C.F., Angione, K., and Milunsky, J.M. (2015). Identification of critical region responsible for split hand/foot malformation type 3 (SHFM3) phenotype through systematic review of literature and mapping of breakpoints using microarray data. Microarrays (Basel) *5*, E2.
10. Nusse, R., and Clevers, H. (2017). Wnt/β-catenin signaling, disease, and emerging therapeutic modalities. Cell *169*, 985–999.
11. Fuchs, S.Y., Chen, A., Xiong, Y., Pan, Z.Q., and Ronai, Z. (1999). HOS, a human homolog of Slimb, forms an SCF complex with Skp1 and Cullin1 and targets the phosphorylation-dependent degradation of IkappaB and beta-catenin. Oncogene *18*, 2039–2046.
12. Fujimura, N. (2016). WNT/β-catenin signaling in vertebrate eye development. Front. Cell Dev. Biol. *4*, 138.
13. Noelanders, R., and Vleminckx, K. (2017). How Wnt signaling builds the brain: Bridging development and disease. Neuroscientist *23*, 314–329.
14. Raspopovic, J., Marcon, L., Russo, L., and Sharpe, J. (2014). Modeling digits. Digit patterning is controlled by a Bmp-Sox9-Wnt Turing network modulated by morphogen gradients. Science *345*, 566–570.
15. Cavodeassi, F., Creuzet, S., and Etchevers, H.C. (2018). The hedgehog pathway and ocular developmental anomalies. Hum. Genet., Epub ahead of print.
16. Al-Qattan, M.M. (2018). Zone of polarizing activity regulatory sequence mutations/duplications with preaxial polydactyly and longitudinal preaxial ray deficiency in the phenotype: A review of human cases, animal models, and insights regarding the pathogenesis. BioMed Res. Int. *2018*, 1573871.
17. Fantes, J., Ragge, N.K., Lynch, S.A., McGill, N.I., Collin, J.R., Howard-Peebles, P.N., Hayward, C., Vivian, A.J., Williamson, K., van Heyningen, V., and FitzPatrick, D.R. (2003). Mutations in SOX2 cause anophthalmia. Nat. Genet. *33*, 461–463.
18. Errichiello, E., Gorgone, C., Giuliano, L., Iadarola, B., Cosentino, E., Rossato, M., Kurtas, N.E., Delledonne, M., Mattina, T., and Zuffardi, O. (2018). SOX2: Not always eye malformations. Severe genital but no major ocular anomalies in a female patient with the recurrent c.70del20 variant. Eur. J. Med. Genet. *61*, 335–340.
19. Jin, J., Cardozo, T., Lovering, R.C., Elledge, S.J., Pagano, M., and Harper, J.W. (2004). Systematic analysis and nomenclature of mammalian F-box proteins. Genes Dev. *18*, 2573–2580.
20. Wu, G., Xu, G., Schulman, B.A., Jeffrey, P.D., Harper, J.W., and Pavletich, N.P. (2003). Structure of a beta-TrCP1-Skp1-beta-catenin complex: Destruction motif binding and lysine specificity of the SCF(beta-TrCP1) ubiquitin ligase. Mol. Cell *11*, 1445–1456.
21. Xu, C., and Min, J. (2011). Structure and function of WD40 domain proteins. Protein Cell *2*, 202–214.
22. El-Hattab, A.W., Dai, H., Almannai, M., Wang, J., Faqeih, E.A., Al Asmari, A., Saleh, M.A.M., Elamin, M.A.O., Alfadhel, M., Alkuraya, F.S., et al. (2017). Molecular and clinical spectra of FBXL4 deficiency. Hum. Mutat. *38*, 1649–1659.
23. Willems, A.R., Schwab, M., and Tyers, M. (2004). A hitchhiker's guide to the cullin ubiquitin ligases: SCF and its kin. Biochim. Biophys. Acta *1695*, 133–170.
24. Petrovski, S., Wang, Q., Heinzen, E.L., Allen, A.S., and Goldstein, D.B. (2013). Genic intolerance to functional variation and the interpretation of personal genomes. PLoS Genet. *9*, e1003709.
25. Samocha, K.E., Robinson, E.B., Sanders, S.J., Stevens, C., Sabo, A., McGrath, L.M., Kosmicki, J.A., Rehnström, K., Mallick, S., Kirby, A., et al. (2014). A framework for the interpretation of de novo mutation in human disease. Nat. Genet. *46*, 944–950.
26. Lek, M., Karczewski, K.J., Minikel, E.V., Samocha, K.E., Banks, E., Fennell, T., O'Donnell-Luria, A.H., Ware, J.S., Hill, A.J., Cummings, B.B., et al.; Exome Aggregation Consortium (2016). Analysis of protein-coding genetic variation in 60,706 humans. Nature *536*, 285–291.
27. De Rubeis, S., He, X., Goldberg, A.P., Poultney, C.S., Samocha, K., Cicek, A.E., Kou, Y., Liu, L., Fromer, M., Walker, S., et al.; DDD Study; Homozygosity Mapping Collaborative for Autism; and UK10K Consortium (2014). Synaptic, transcriptional and chromatin genes disrupted in autism. Nature *515*, 209–215.
28. Iossifov, I., O'Roak, B.J., Sanders, S.J., Ronemus, M., Krumm, N., Levy, D., Stessman, H.A., Witherspoon, K.T., Vives, L., Patterson, K.E., et al. (2014). The contribution of de novo coding mutations to autism spectrum disorder. Nature *515*, 216–221.
29. Cooper, G.M., Stone, E.A., Asimenos, G., Green, E.D., Batzoglou, S., Sidow, A.; and NISC Comparative Sequencing Program (2005). Distribution and intensity of constraint in mammalian genomic sequence. Genome Res. *15*, 901–913.
30. Davydov, E.V., Goode, D.L., Sirota, M., Cooper, G.M., Sidow, A., and Batzoglou, S. (2010). Identifying a high fraction of the human genome to be under selective constraint using GERP++. PLoS Comput. Biol. *6*, e1001025.
31. Havrilla, J.M., Pedersen, B.S., Layer, R.M., and Quinlan, A.R. (2019). A map of constrained coding regions in the human genome. Nat. Genet. *51*, 88–95.
32. Berman, H.M., Westbrook, J., Feng, Z., Gilliland, G., Bhat, T.N., Weissig, H., Shindyalov, I.N., and Bourne, P.E. (2000). The Protein Data Bank. Nucleic Acids Res. *28*, 235–242.
33. Motta, M., Fidan, M., Bellacchio, E., Pantaleoni, F., Schneider-Heieck, K., Coppola, S., Borck, G., Salviati, L., Zenker, M., Cirstea, I.C., et al. (2019). Dominant Noonan syndrome-causing LZTR1 mutations specifically affect the kelch domain substrate-recognition surface and enhance RAS-MAPK signaling. Hum. Mol. Genet *28*, 1007–1022.

34. Lelieveld, S.H., Wiel, L., Venselaar, H., Pfundt, R., Vriend, G., Veltman, J.A., Brunner, H.G., Vissers, L.E.L.M., and Gilissen, C. (2017). Spatial clustering of de novo missense mutations identifies candidate neurodevelopmental disorder-associated genes. Am. J. Hum. Genet. *101*, 478–484.
35. Schymkowitz, J., Borg, J., Stricher, F., Nys, R., Rousseau, F., and Serrano, L. (2005). The FoldX web server: An online force field. Nucleic Acids Res. *33*, W382-8.
36. Lai, C.S., Gerrelli, D., Monaco, A.P., Fisher, S.E., and Copp, A.J. (2003). FOXP2 expression during brain development coincides with adult sites of pathology in a severe speech and language disorder. Brain *126*, 2455–2462.
37. Morais da Silva, S., Hacker, A., Harley, V., Goodfellow, P., Swain, A., and Lovell-Badge, R. (1996). Sox9 expression during gonadal development implies a conserved role for the gene in testis differentiation in mammals and birds. Nat. Genet. *14*, 62–68.
38. Hooper, J.E., and Scott, M.P. (2005). Communicating with Hedgehogs. Nat. Rev. Mol. Cell Biol. *6*, 306–317.
39. Aldinger, K.A., Mendelsohn, N.J., Chung, B.H., Zhang, W., Cohn, D.H., Fernandez, B., Alkuraya, F.S., Dobyns, W.B., and Curry, C.J. (2016). Variable brain phenotype primarily affects the brainstem and cerebellum in patients with osteogenesis imperfecta caused by recessive WNT1 mutations. J. Med. Genet. *53*, 427–430.
40. Thisse, C., and Thisse, B. (2008). High-resolution in situ hybridization to whole-mount zebrafish embryos. Nat. Protoc. *3*, 59–69.
41. El-Brolosy, M.A., Kontarakis, Z., Rossi, A., Kuenne, C., Günther, S., Fukuda, N., Kikhi, K., Boezio, G.L.M., Takacs, C.M., Lai, S.L., et al. (2019). Genetic compensation triggered by mutant mRNA degradation. Nature *568*, 193–197.
42. El-Brolosy, M.A., and Stainier, D.Y.R. (2017). Genetic compensation: A phenomenon in search of mechanisms. PLoS Genet. *13*, e1006780.
43. Rossi, A., Kontarakis, Z., Gerri, C., Nolte, H., Hölper, S., Krüger, M., and Stainier, D.Y. (2015). Genetic compensation induced by deleterious mutations but not gene knockdowns. Nature *524*, 230–233.
44. Aberle, H., Bauer, A., Stappert, J., Kispert, A., and Kemler, R. (1997). beta-catenin is a target for the ubiquitin-proteasome pathway. EMBO J. *16*, 3797–3804.
45. Kim, C.H., Oda, T., Itoh, M., Jiang, D., Artinger, K.B., Chandrasekharappa, S.C., Driever, W., and Chitnis, A.B. (2000). Repressor activity of Headless/Tcf3 is essential for vertebrate head formation. Nature *407*, 913–916.
46. Heisenberg, C.P., Houart, C., Take-Uchi, M., Rauch, G.J., Young, N., Coutinho, P., Masai, I., Caneparo, L., Concha, M.L., Geisler, R., et al. (2001). A mutation in the Gsk3-binding domain of zebrafish Masterblind/Axin1 leads to a fate transformation of telencephalon and eyes to diencephalon. Genes Dev. *15*, 1427–1434.
47. Young, R.M., Hawkins, T.A., Cavodeassi, F., Stickney, H.L., Schwarz, Q., Lawrence, L.M., Wierzbicki, C., Cheng, B.Y., Luo, J., Ambrosio, E.M., et al. (2019). Compensatory growth renders Tcf7l1a dispensable for eye formation despite its requirement in eye field specification. eLife *8*, e40093.
48. Hurlstone, A.F., Haramis, A.P., Wienholds, E., Begthel, H., Korving, J., Van Eeden, F., Cuppen, E., Zivkovic, D., Plasterk, R.H., and Clevers, H. (2003). The Wnt/beta-catenin pathway regulates cardiac valve formation. Nature *425*, 633–637.
49. Kennerson, M.L., Warburton, T., Nelis, E., Brewer, M., Polly, P., De Jonghe, P., Timmerman, V., and Nicholson, G.A. (2007). Mutation scanning the GJB1 gene with high-resolution melting analysis: implications for mutation scanning of genes for Charcot-Marie-Tooth disease. Clin. Chem. *53*, 349–352.
50. Stamos, J.L., and Weis, W.I. (2013). The β-catenin destruction complex. Cold Spring Harb. Perspect. Biol. *5*, a007898.
51. Winston, J.T., Strack, P., Beer-Romero, P., Chu, C.Y., Elledge, S.J., and Harper, J.W. (1999). The SCFbeta-TRCP-ubiquitin ligase complex associates specifically with phosphorylated destruction motifs in IkappaBalpha and beta-catenin and stimulates IkappaBalpha ubiquitination in vitro. Genes Dev. *13*, 270–283.
52. Li, Y., Pawlik, B., Elcioglu, N., Aglan, M., Kayserili, H., Yigit, G., Percin, F., Goodman, F., Nürnberg, G., Cenani, A., et al. (2010). LRP4 mutations alter Wnt/beta-catenin signaling and cause limb and kidney malformations in Cenani-Lenz syndrome. Am. J. Hum. Genet. *86*, 696–706.
53. Hoseth, E.Z., Krull, F., Dieset, I., Mørch, R.H., Hope, S., Gardsjord, E.S., Steen, N.E., Melle, I., Brattbakk, H.R., Steen, V.M., et al. (2018). Exploring the Wnt signaling pathway in schizophrenia and bipolar disorder. Transl. Psychiatry *8*, 55.
54. Martinez, G., Wijesinghe, M., Turner, K., Abud, H.E., Taketo, M.M., Noda, T., Robinson, M.L., and de Iongh, R.U. (2009). Conditional mutations of beta-catenin and APC reveal roles for canonical Wnt signaling in lens differentiation. Invest. Ophthalmol. Vis. Sci. *50*, 4794–4806.
55. Alldredge, A., and Fuhrmann, S. (2016). Loss of Axin2 causes ocular defects during mouse eye development. Invest. Ophthalmol. Vis. Sci. *57*, 5253–5262.
56. Carter, T.C., Sicko, R.J., Kay, D.M., Browne, M.L., Romitti, P.A., Edmunds, Z.L., Liu, A., Fan, R., Druschel, C.M., Caggana, M., et al. (2017). Copy-number variants and candidate gene mutations in isolated split hand/foot malformation. J. Hum. Genet. *62*, 877–884.
57. Jiang, J., and Struhl, G. (1998). Regulation of the Hedgehog and Wingless signalling pathways by the F-box/WD40-repeat protein Slimb. Nature *391*, 493–496.
58. Milétich, I., and Limbourg-Bouchon, B. (2000). Drosophila null slimb clones transiently deregulate Hedgehog-independent transcription of wingless in all limb discs, and induce decapentaplegic transcription linked to imaginal disc regeneration. Mech. Dev. *93*, 15–26.
59. Skwarek, L.C., Windler, S.L., de Vreede, G., Rogers, G.C., and Bilder, D. (2014). The F-box protein Slmb restricts the activity of aPKC to polarize epithelial cells. Development *141*, 2978–2983.
60. Johnson, D.R. (1967). Extra-toes: A new mutant gene causing multiple abnormalities in the mouse. J. Embryol. Exp. Morphol. *17*, 543–581.
61. Franz, T., and Besecke, A. (1991). The development of the eye in homozygotes of the mouse mutant Extra-toes. Anat. Embryol. (Berl.) *184*, 355–361.
62. Furimsky, M., and Wallace, V.A. (2006). Complementary Gli activity mediates early patterning of the mouse visual system. Dev. Dyn. *235*, 594–605.
63. Hui, C.C., and Joyner, A.L. (1993). A mouse model of greig cephalopolysyndactyly syndrome: The extra-toesJ mutation contains an intragenic deletion of the Gli3 gene. Nat. Genet. *3*, 241–246.
64. Bakrania, P., Efthymiou, M., Klein, J.C., Salt, A., Bunyan, D.J., Wyatt, A., Ponting, C.P., Martin, A., Williams, S., Lindley, V.,

et al. (2008). Mutations in BMP4 cause eye, brain, and digit developmental anomalies: Overlap between the BMP4 and hedgehog signaling pathways. Am. J. Hum. Genet. *82*, 304–319.
65. Bakrania, P., Ugur Iseri, S.A., Wyatt, A.W., Bunyan, D.J., Lam, W.W., Salt, A., Ramsay, J., Robinson, D.O., and Ragge, N.K. (2010). Sonic hedgehog mutations are an uncommon cause of developmental eye anomalies. Am. J. Med. Genet. A. *152A*, 1310–1313.
66. Chassaing, N., Davis, E.E., McKnight, K.L., Niederriter, A.R., Causse, A., David, V., Desmaison, A., Lamarre, S., Vincent-Delorme, C., Pasquier, L., et al. (2016). Targeted resequencing identifies PTCH1 as a major contributor to ocular developmental anomalies and extends the SOX2 regulatory network. Genome Res. *26*, 474–485.
67. Roessler, E., Du, Y.Z., Mullor, J.L., Casas, E., Allen, W.P., Gillessen-Kaesbach, G., Roeder, E.R., Ming, J.E., Ruiz i Altaba, A., and Muenke, M. (2003). Loss-of-function mutations in the human GLI2 gene are associated with pituitary anomalies and holoprosencephaly-like features. Proc. Natl. Acad. Sci. USA *100*, 13424–13429.
68. Rahimov, F., Ribeiro, L.A., de Miranda, E., Richieri-Costa, A., and Murray, J.C. (2006). GLI2 mutations in four Brazilian patients: How wide is the phenotypic spectrum? Am. J. Med. Genet. A. *140*, 2571–2576.
69. Johnston, J.J., Sapp, J.C., Turner, J.T., Amor, D., Aftimos, S., Aleck, K.A., Bocian, M., Bodurtha, J.N., Cox, G.F., Curry, C.J., et al. (2010). Molecular analysis expands the spectrum of phenotypes associated with GLI3 mutations. Hum. Mutat. *31*, 1142–1154.
70. Bertolacini, C.D.P., Ribeiro-Bicudo, L.A., Petrin, A., Richieri-Costa, A., and Murray, J.C. (2012). Clinical findings in patients with GLI2 mutations–phenotypic variability. Clin. Genet. *81*, 70–75.
71. Roberts, A.E., Allanson, J.E., Tartaglia, M., and Gelb, B.D. (2013). Noonan syndrome. Lancet *381*, 333–342.
72. Tartaglia, M., and Gelb, B.D. (2010). Disorders of dysregulated signal traffic through the RAS-MAPK pathway: Phenotypic spectrum and molecular mechanisms. Ann. N Y Acad. Sci. *1214*, 99–121.
73. de la Vega, M., Burrows, J.F., and Johnston, J.A. (2011). Ubiquitination: Added complexity in Ras and Rho family GTPase function. Small GTPases *2*, 192–201.
74. Steklov, M., Pandolfi, S., Baietti, M.F., Batiuk, A., Carai, P., Najm, P., Zhang, M., Jang, H., Renzi, F., Cai, Y., et al. (2018). Mutations in LZTR1 drive human disease by dysregulating RAS ubiquitination. Science *362*, 1177–1182.
75. Bigenzahn, J.W., Collu, G.M., Kartnig, F., Pieraks, M., Vladimer, G.I., Heinz, L.X., Sedlyarov, V., Schischlik, F., Fauster, A., Rebsamen, M., et al. (2018). LZTR1 is a regulator of RAS ubiquitination and signaling. Science *362*, 1171–1177.
76. Kim, S.E., Yoon, J.Y., Jeong, W.J., Jeon, S.H., Park, Y., Yoon, J.B., Park, Y.N., Kim, H., and Choi, K.Y. (2009). H-Ras is degraded by Wnt/beta-catenin signaling via beta-TrCP-mediated polyubiquitylation. J. Cell Sci. *122*, 842–848.
77. Li, Q., and Wang, K. (2017). InterVar: Clinical interpretation of genetic variants by the 2015 ACMG-AMP guidelines. Am. J. Hum. Genet. *100*, 267–280.
78. Ng, P.C., and Henikoff, S. (2003). SIFT: Predicting amino acid changes that affect protein function. Nucleic Acids Res. *31*, 3812–3814.
79. Adzhubei, I.A., Schmidt, S., Peshkin, L., Ramensky, V.E., Gerasimova, A., Bork, P., Kondrashov, A.S., and Sunyaev, S.R. (2010). A method and server for predicting damaging missense mutations. Nat. Methods *7*, 248–249.

The American Journal of Human Genetics, Volume *105*

Supplemental Data

De Novo Missense Variants in *FBXW11* Cause Diverse Developmental Phenotypes Including Brain, Eye, and Digit Anomalies

Richard J. Holt, Rodrigo M. Young, Berta Crespo, Fabiola Ceroni, Cynthia J. Curry, Emanuele Bellacchio, Dorine A. Bax, Andrea Ciolfi, Marleen Simon, Christina R. Fagerberg, Ellen van Binsbergen, Alessandro De Luca, Luigi Memo, William B. Dobyns, Alaa Afif Mohammed, Samuel J.H. Clokie, Celia Zazo Seco, Yong-Hui Jiang, Kristina P. Sørensen, Helle Andersen, Jennifer Sullivan, Zöe Powis, Anna Chassevent, Constance Smith-Hicks, Slavé Petrovski, Thalia Antoniadi, Vandana Shashi, Bruce D. Gelb, Stephen W. Wilson, Dianne Gerrelli, Marco Tartaglia, Nicolas Chassaing, Patrick Calvas, and Nicola K. Ragge

Supplemental Data

Supplemental Note: Case Reports

Individual 1 was born with bilateral eye anomalies following an uncomplicated pregnancy. At 13 years-of-age, she had right microphthalmia (17.4 mm axial length) with a small anterior segment (horizontal corneal diameter [HCD] 5 mm), iris coloboma, absent lens, a large chorioretinal coloboma and persistent hyaloid vessel with no perception of light. Her left eye had an axial length of 20.4 mm (low borderline normal) with small anterior segment (HCD 6.5 mm), iris coloboma, thin lens, and large chorioretinal coloboma and a visual acuity of 2/60 (corrected with 0.00, -2.25 D x 100). She had mild retrognathia, wide sandal gaps between 1^{st} and 2^{nd} toes, left 2-3 toe syndactyly, mesoaxial polydactyly of the left 3^{rd} toe (surgically corrected), contractures of the left 4^{th} and 5^{th} toes, and contractures of the left 4^{th} and 5^{th} fingers. Her overall development was normal, although she had some psychiatric issues during adolescence and early adulthood. No other candidate variants to potentially explain the patient's phenotype were identified by whole exome sequencing (WES) or array comparative genomic hybridisation (aCGH).

Individual 2 was a 9-year-old boy with global developmental delay. He was born following an uneventful pregnancy at full term by caesarean section, following a prolonged labour. He had infantile strabismus that resolved, delayed motor, cognitive and speech development. He walked at age 3 years and talked in single words at 5½-6 years. At age 9 years, his general development was around the 4-year-old level. He spoke only in short phrases and he had behavioural issues with a preference for strict routine, frustration with lack of communication and self-injurious behaviours. He had a prominent glabella, a broad, possibly bifid uvula, retrognathia, and a prominent nasal tip. He had a right transverse

palmar crease, mildly short 5th metacarpals, relatively short digits, slightly thin thumbs with deficiency of thenar and hypothenar muscle eminencies bilaterally. He had wide spaces between all of his toes with contractures of the 2nd and 4th toes, short 5th metatarsals, lateral clinodactyly of the 2nd toe, which was moderately broad, and mild 2-3 toe syndactyly. He walked with a slightly unusual gait and tended to toe walk. His deep tendon reflexes were brisk. MRI revealed a severely abnormal corpus callosum with absent splenium, thick Probst bundles, small globular dysplastic hippocampi and mildly reduced white matter volume. No other variants of interest were identified in this individual by WES.

Individual 3, in addition to the *de novo* missense variant in *FBXW11*, carried two paternally inherited heterozygous mutations, in *GALT* (MIM: 230400) and *PTS* (MIM: 261640), predicted pathogenic, but with no evidence of a second mutation in either or phenotypes matching the known recessive disorders associated with variants in these genes. SNP array analysis was normal, and there was no CGG repeat expansion in *FMR1* (MIM: 309550). Individual 3 was the second child of non-consanguineous parents. Pregnancy and birth were unremarkable. His development was delayed. He started walking at the age of 20 months, and toe walked for a long time. His first words came at the age of one year; however, after 1 – 1.5 years there was stagnation or even regression in his language skills. He never combined words and is practically nonverbal as an adult. He was diagnosed with classic autism and severe intellectual disability and showed compulsive behaviour. At 23 years, he was emotionally at the level of 18 months. His hearing and vision were normal, with mild myopia. He had normal growth parameters and no dysmorphic features.

Individual 4 had extreme microcephaly (congenital), very small stature and a history of global developmental delay with moderate/severe intellectual disability (ID) and absent speech. Pregnancy and birth were unremarkable. She exhibited some stereotypies with her hands and self-injurious behaviour. She had dysmorphic facial features including micrognathia, tall sloping forehead, malar hypoplasia, long, smooth philtrum, bifid nasal tip, thin upper lip, small ears and mild ptosis, with normal external eye appearances. She exhibited digital anomalies, with shortening of the distal phalanx of the thumbs and big toes, bilateral 5th finger clinodactyly, thenar hypoplasia on the right and mild thenar hypoplasia on the left, and increased curvature of thumb and all toenails, indicative of distal digital hypoplasia. In addition to the variant in *FBXW11*, variants of unknown clinical significance in two additional genes were noted. A *de novo* missense change (NM_152486.2:c.58A>G, NP_689699.2:p.Ile20Val) was identified in *SAMD11* (MIM: 616765), while inherited compound heterozygous variants were present in *SYCP2L* (MIM: 616799) (NM_001040274.2:c.1720G>A, NP_001035364.2:p.Glu574Lys, maternally inherited; NM_001040274.2:c.1777G>C, NP_001035364.2:p.Ala593Pro, paternally inherited). Array CGH analysis was normal.

Individual 5 was a 1-year-old girl born with a severe pulmonary stenosis (operated on at a few days of age), unilateral (right) renal hypoplasia with compensatory left renal hypertrophy, renovascular hypertension and adducted thumbs. She had a broad nasal bridge, short nose, deep philtrum, and retrognathia. Her feet showed no anomalies. Her eye examination was unremarkable apart from alternating exotropia. At a few days of age she suffered a circulation collapse. She has been clinically diagnosed with cerebral palsy. Cerebral MRI at age 10 months showed generalised white matter atrophy and small

periventricular changes in white matter with discrete hemosiderin deposits indicating a small haemorrhagic component at some point earlier in life. At age 6 months, her development was delayed corresponding to approximately age 3 months. At 8 months she recognised her parents and smiled. At 1 year she could hold her head, but was unable to roll or sit. In addition to the *FBXW11* variant, the girl carried another *de novo* variant in *OLFML3* (MIM: 610088) (NM_020190 c.398C>T, p.Thr133Ile, chr1:114,523,237), absent from gnomAD and of uncertain clinical significance. Array CGH (Affymetrix Cytoscan HD) did not reveal any potentially pathogenic structural variant.

Individual 6 was an 8 year old boy with macrocephaly, intellectual disability, autism spectrum disorder and hypotonia. He was born at 38 weeks' gestation with a birth weight of 3.4kg following a pregnancy complicated by gestational diabetes and cervical incompetence, treated with Pitocon. His birth history was otherwise unremarkable. His motor development was slightly delayed: he sat at 9 months, walked at 18 months. His speech was also delayed, with first words at 2 years, and combining words at 3 years. He was able to feed himself with a spoon at 1 year old and developed a mature pincer at 3 years old. At the time of last assessment, he continued to have poor coordination and difficulty with motor planning and completing tasks without direct supervision. He had particular difficulty with attention and behaviour management. Full scale IQ (FSIQ) at 7 years old was in the Extremely Low Range between 61-72 (average between 90-109). Verbal comprehension was normal. MRI indicated he had mild prominence of the lateral ventricles with a mild colpocephalic configuration. He was also noted to have dermal melanosis and cupped ears. No other dysmorphic features were observed. In addition to his *FBXW11* variant, Individual 6 carried a maternally inherited 2q13 duplication (chr2:110,863,908-110,980,346, hg19) also present

in healthy individuals, detected by aCGH using the Human OMNI ExpressExome Beadchip containing over 950,000 markers (Illumina, Inc. USA), and analysed with CNV partition 2.4.4.0. He also had a *MT-ND1* (MIM: 516000) variant that is only 2% heteroplasmy. Neither variant was considered likely to contribute to his phenotype.

Individual 7 was born following an uneventful pregnancy at 38 weeks. Bilateral cryptorchidism was noticed at birth. At age 13 months, he exhibited macrocephaly, dysmorphic facial features including frontal bossing, deep broad nasal bridge, epicanthus, low-set posteriorly rotated ears, large and protruding tongue, webbed neck, and pectus carinatum. He showed disproportionate short stature as well as small hands and feet. He had bilateral clinodactyly of the fourth and fifth toes, with the second toe overlapping the first. He had a flat angioma on the median nuchal region, a nevus on the right buttock, and a cafè-au-lait spot on the right leg. MRI documented agenesis of the corpus callosum with only evidence of the genu, prominence of lateral ventricles with mild colpocephalic configuration. Echocardiography showed a patent foramen ovale. At subsequent examinations, he displayed an accentuation of macrocephaly and mild prognathism with dental malocclusion, reduced growth, thoracolumbar scoliosis, and a supernumerary rib. He had delayed motor, cognitive and speech development. He walked independently at 3 years, and spoke his first words at 2 years. Currently he is in elementary school, requiring learning support. He lacks anal sphincter control, shows a self-injurious, impulsive and aggressive behaviour, and has sleep difficulties. Based on the presence of clinical features that were suggestive of Noonan syndrome or a related RASopathy, he was tested for mutations in *PTPN11* (MIM: 176876), *SOS1* (MIM: 182530), *KRAS* (MIM: 190070), *HRAS* (MIM: 190020), *NRAS* (MIM: 164790), *SHOC2* (MIM: 602775), *BRAF* (MIM: 164757), *RAF1*

(MIM: 164760), *MAP2K1* (MIM: 176872), *MAP2K2* (MIM: 601263), *RIT1* (MIM: 609591) and *CBL* (MIM: 165360), which yielded negative results. Karyotype and aCGH analysis did not show any clinically relevant rearrangement. No other potentially causative variants were identified.

Supplemental Figures

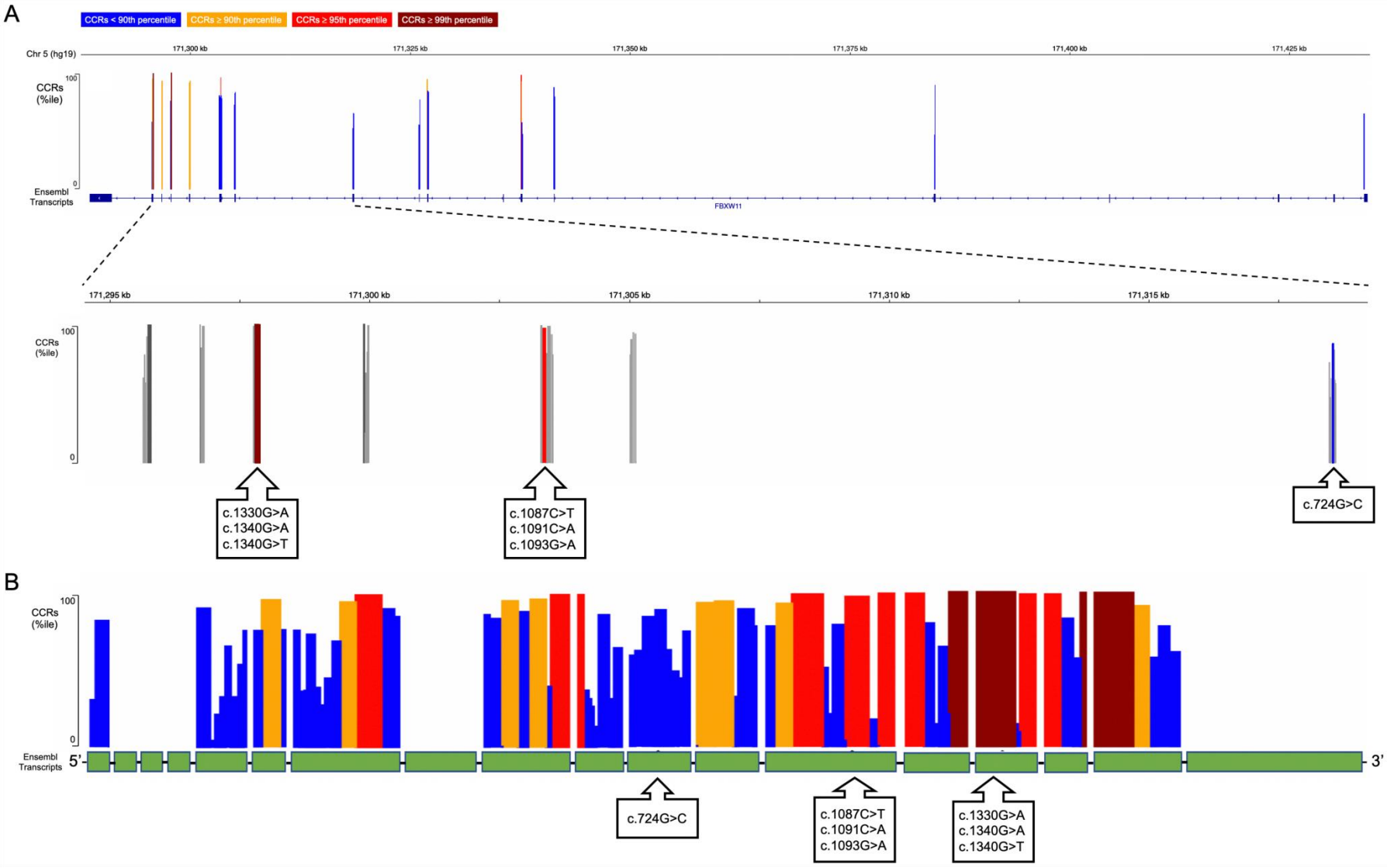

Figure S1: Constrained coding regions (CCRs) within *FBXW11* and locations of the seven missense variants identified in this study. The diagrams show the *FBXW11* gene and cDNA structure (Ensembl Gene ID: ENSG00000072803; Transcript ID: ENST00000265094), where the coding exons from all isoforms are combined in a single model of coding sequence according to the model developed by Havrilla *et al*.[1] CCRs ranking at the highest percentiles represent the protein-coding regions under the highest constraint in the human genome. A: CCRs are reported as histogram bars on the corresponding genomic regions. The height of the bars and their colours indicate predicted constraint as percentile ranking (top). The underlying inset shows an enlargement of the genomic region containing the identified variants. The corresponding CCRs are highlighted as above. Specifically, the three CCRs harbouring the missense variants identified in this study have the following genomic boundaries: chr5:171,318,530-171,318,553 (rank: 85th percentile, amino acid 242); chr5:171,303,339-171,303,385 (rank: 96th percentile, amino acids 363 – 365); chr5:171,297,790-171,297,862 (rank: 99th percentile, amino acids 444 – 447). B: Histograms bars showing ranking of CCRs are depicted along the *FBXW11* coding sequence, according to the same scheme as panel A. Green boxes indicate coding exons.

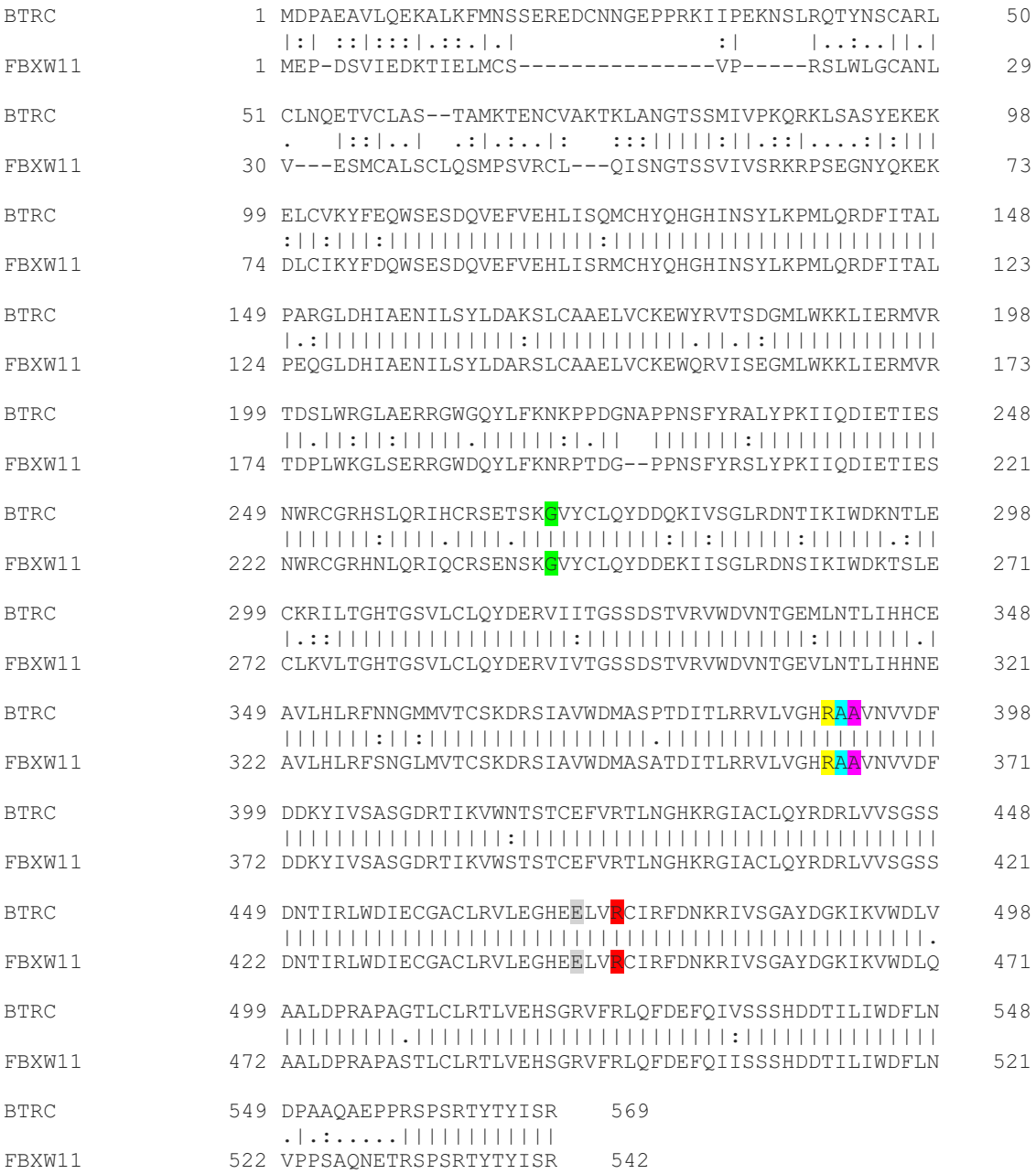

Figure S2: EMBOSS Needle alignment of BTRC (NP_003930.1) and FBXW11 (NP_036432.2).

The positions of the missense variants identified in *FBXW11* are indicated: green = p.Gly242Arg, yellow = p.Arg363Trp, blue = p.Ala364Asp, purple = p.Ala365Thr, grey = p.Glu444Lys, red = p.Arg447Gln/p.Arg447Leu.

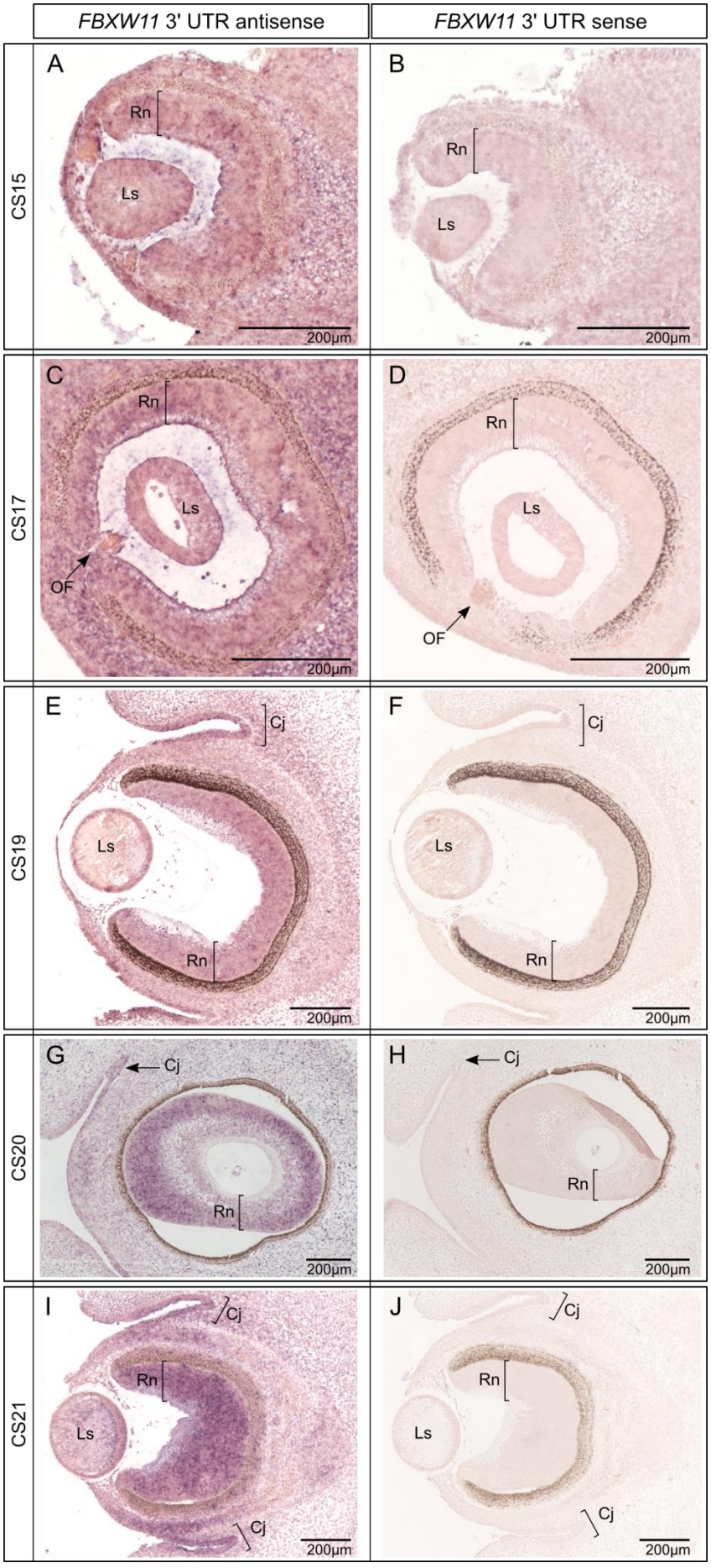
FBXW11 3' UTR antisense
FBXW11 3' UTR sense
CS15
CS17
CS19
CS20
CS21
A
B
C
D
E
F
G
H
I
J
Rn
Ls
OF
Cj
200µm

Figure S3: *In situ* hybridisation studies using the 3' UTR probe showing *FBXW11* expression during human eye development. *In situ* hybridisations of sagittal sections of the eye at CS15 (A,B), CS17 (C,D), CS19 (E,F), CS20 (G,H) and CS21 (I,J) using *FBXW11* 3' UTR antisense (left panel) and sense (right panel) probes. *FBXW11* signal was present in the lens (A, C, E, I), the retina (A, C, E, G, I), lips of the optic fissure closure (C) and regions of the conjunctiva (E, G, I). *Abbreviations*: Cj, Conjunctiva; Ls, Lens; OF, Optic Fissure; Rn, Retina.

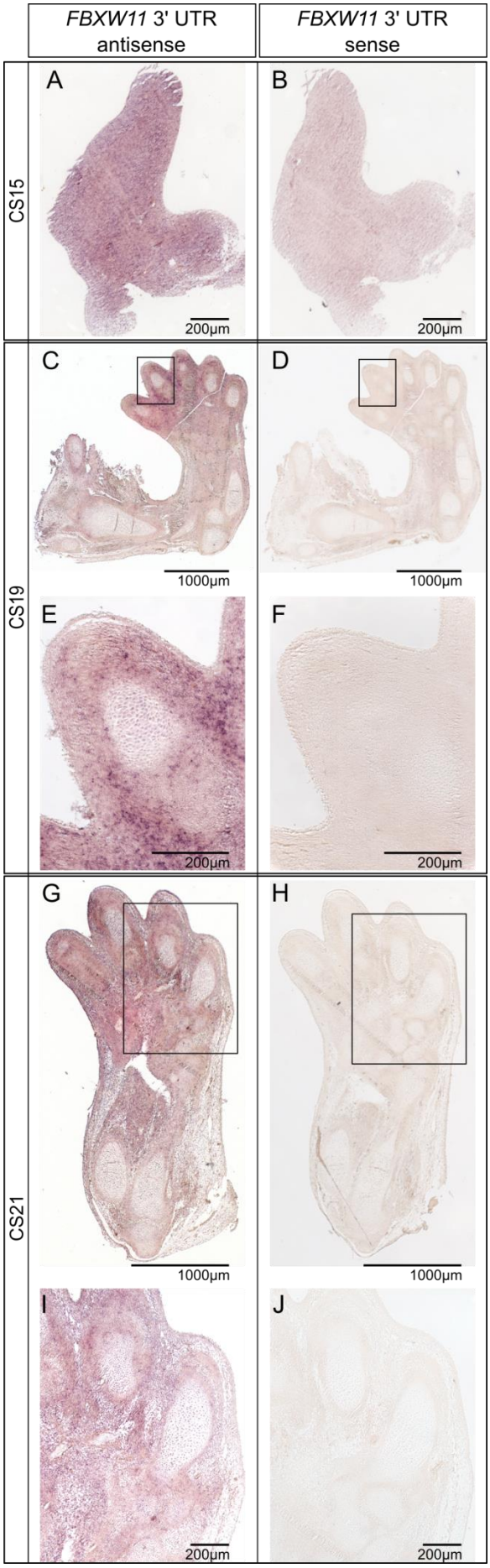
FBXW11 3' UTR antisense
FBXW11 3' UTR sense
CS15
CS19
CS21
A
B
C
D
E
F
G
H
I
J
200µm
1000µm

Figure S4: *In situ* hybridisation studies using the 3' UTR probe showing *FBXW11* expression during human limb development. *In situ* hybridisations of coronal sections of the forelimb at different CS stages, using *FBXW11* 3' UTR antisense (left panel) and sense (right panel) probes. E, F, I, J show increased magnification of the boxed regions at CS19 (C, D) and CS21 (G, H), highlighting *FBXW11* expression around the developing cartilage of the digits in the hand plate (E, I).

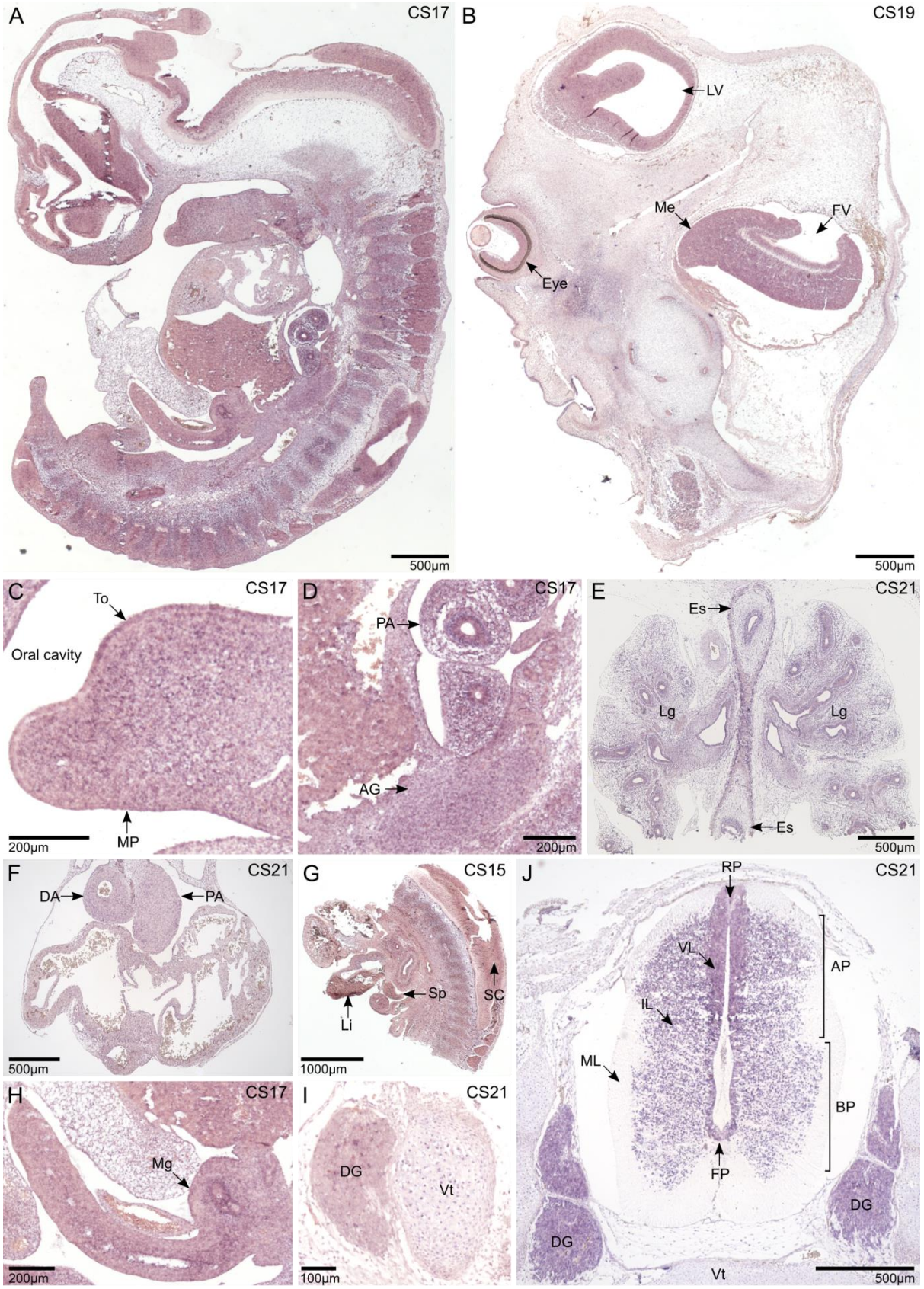
A
CS17
500μm
B
CS19
LV
Me
FV
Eye
500μm
C
CS17
To
Oral cavity
MP
200μm
D
CS17
PA
AG
200μm
E
CS21
Es
Lg
Lg
Es
500μm
F
CS21
DA
PA
500μm
G
CS15
Sp
SC
Li
1000μm
J
CS21
RP
VL
AP
IL
ML
BP
FP
DG
DG
Vt
500μm
H
CS17
Mg
200μm
I
CS21
DG
Vt
100μm

Figure S5: *In situ* hybridisation studies of *FBXW11* using the 3' UTR antisense probe showing the expression pattern in multiple human embryonic structures. Structures of interest are indicated by arrows. Sagittal section of embryo at CS17 (week 6), showing *FBXW11* expression in multiple developing structures (A). Sagittal section of the head at CS19 (week 7) indicating expression in structures forming the lateral and fourth ventricles, including the metencephalon (B). Increased magnification from (A) of the pharyngeal arches (C), showing a generalised expression in this structure, including the mandibular process and the tongue. Increased magnification from (A) highlighting *FBXW11* expression in the adrenal glands and the pulmonary artery (D). Coronal section CS21 (week 8) showing expression in the lungs (E). Coronal section of the heart at CS21 showing *FBXW11* expression in the dorsal aorta and the pulmonary artery (F). Sagittal section of the embryo at CS15 (week 5) highlighting strong *FBXW11* expression in the liver, spleen and spinal cord (G). Increased magnification from (A), showing *FBXW11* expression in midgut (H). Transverse section at CS21 showing *FBXW11* expression in the dorsal ganglia (I). Transverse section of the spinal cord at CS21 highlighting *FBXW11* expression in the floor plate, roof plate, and the ventricular and the intermediate layers (J). *Abbreviations*: AG, Adrenal Glands; AP, Alar Plate; BP, Basal Plate; DA, Dorsal Aorta; DG, Dorsal Ganglia; Es, Esophagus; FP, Floor Plate; FV, Fourth Ventricle; Hp, Hypothalamus; IL, Intermediate Layer; Lg, Lungs; Li, Liver; LV, Lateral Ventricle; Md, Medulla; Me, Metencephalon; Mg, Midgut; ML, Marginal Layer; MP, Mandibular Process; PA, Pulmonary Artery; RP, Roof Plate; SC, Spinal Cord; Sp, Spleen; To, Tongue; TV, Third ventricle; VL, Ventricular Layer; Vt, Vertebra.

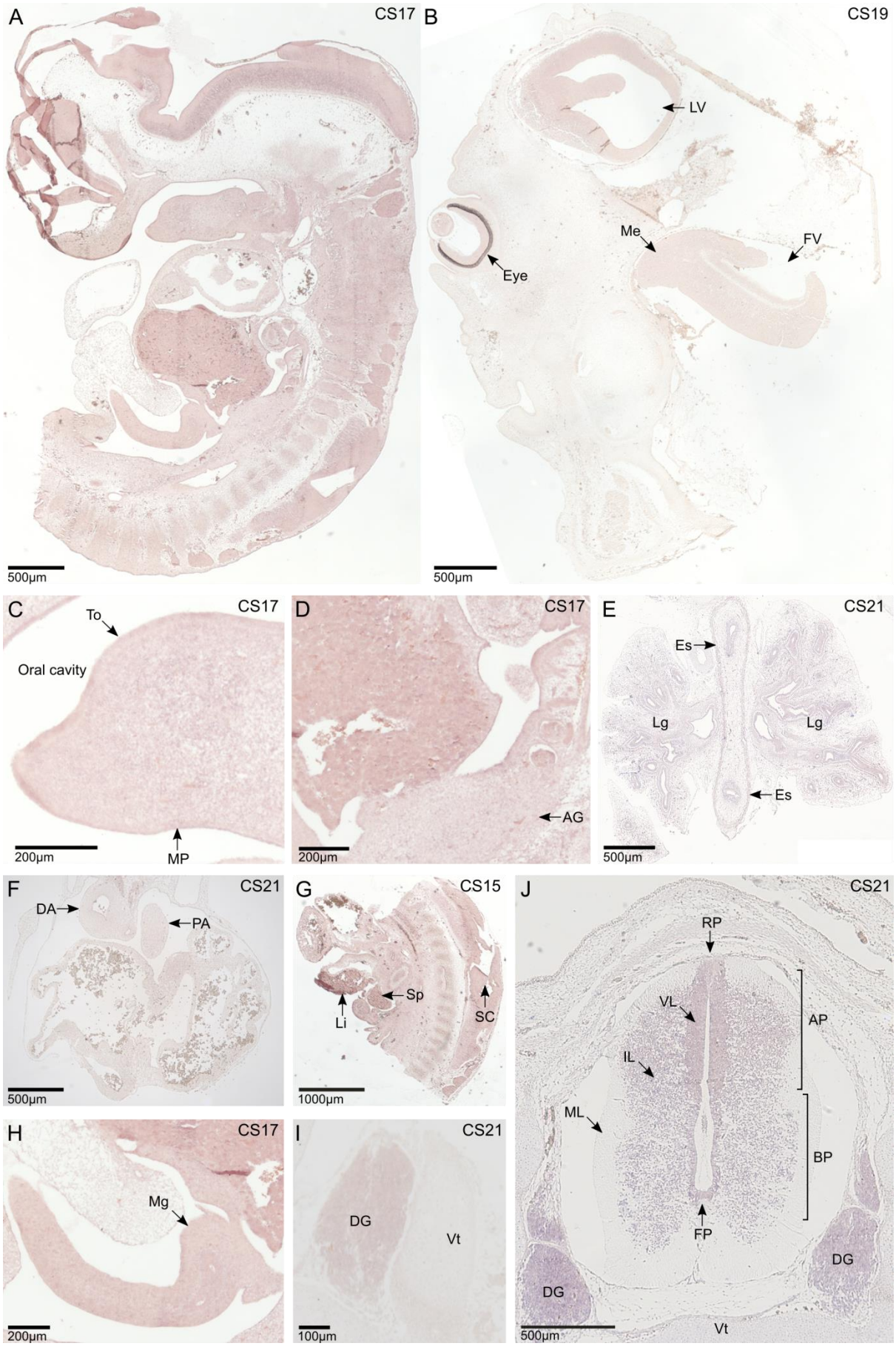
A
CS17
500μm
B
CS19
LV
Me
FV
Eye
500μm
C
CS17
To
Oral cavity
MP
200μm
D
CS17
AG
200μm
E
CS21
Es
Lg
Lg
Es
500μm
F
CS21
DA
PA
500μm
G
CS15
Sp
Li
SC
1000μm
J
CS21
RP
VL
AP
IL
ML
BP
FP
DG
DG
Vt
500μm
H
CS17
Mg
200μm
I
CS21
DG
Vt
100μm

Figure S6: *In situ* hybridisation studies of *FBXW11* 3' UTR sense probe in multiple human embryonic structures. Sagittal section of embryo at CS17 (A). Sagittal section of the head at CS19 (B). Increased magnification of structures from (A): pharyngeal arches (C), including the mandibular process and the tongue, and the adrenal glands (D). Coronal section of the lungs at CS21 (E). Coronal section of the dorsal aorta and the pulmonary artery at CS21 (F). Sagittal section of the embryo at CS15 showing the liver, spleen and spinal cord (G). Increased magnification of (A), showing midgut (H). Transverse section of the dorsal ganglia and developing vertebra at CS21 (I). Transverse section of the spinal cord at CS21 (J). *Abbreviations*: AG, Adrenal Glands; AP, Alar Plate; BP, Basal Plate; DA, Dorsal Aorta; DG, Dorsal Ganglia; Es, Esophagus; FP, Floor Plate; FV, Fourth Ventricle; IL, Intermediate Layer; Lg, Lungs; LV, Lateral Ventricle; Me, Metencephalon; Mg, Midgut; ML, Marginal Layer; MP, Mandibular Process; PA, Pulmonary Artery; RP, Roof Plate; SC, Spinal Cord; Sp, Spleen; To, Tongue; TV, Third ventricle; VL, Ventricular Layer; Vt, Vertebra.

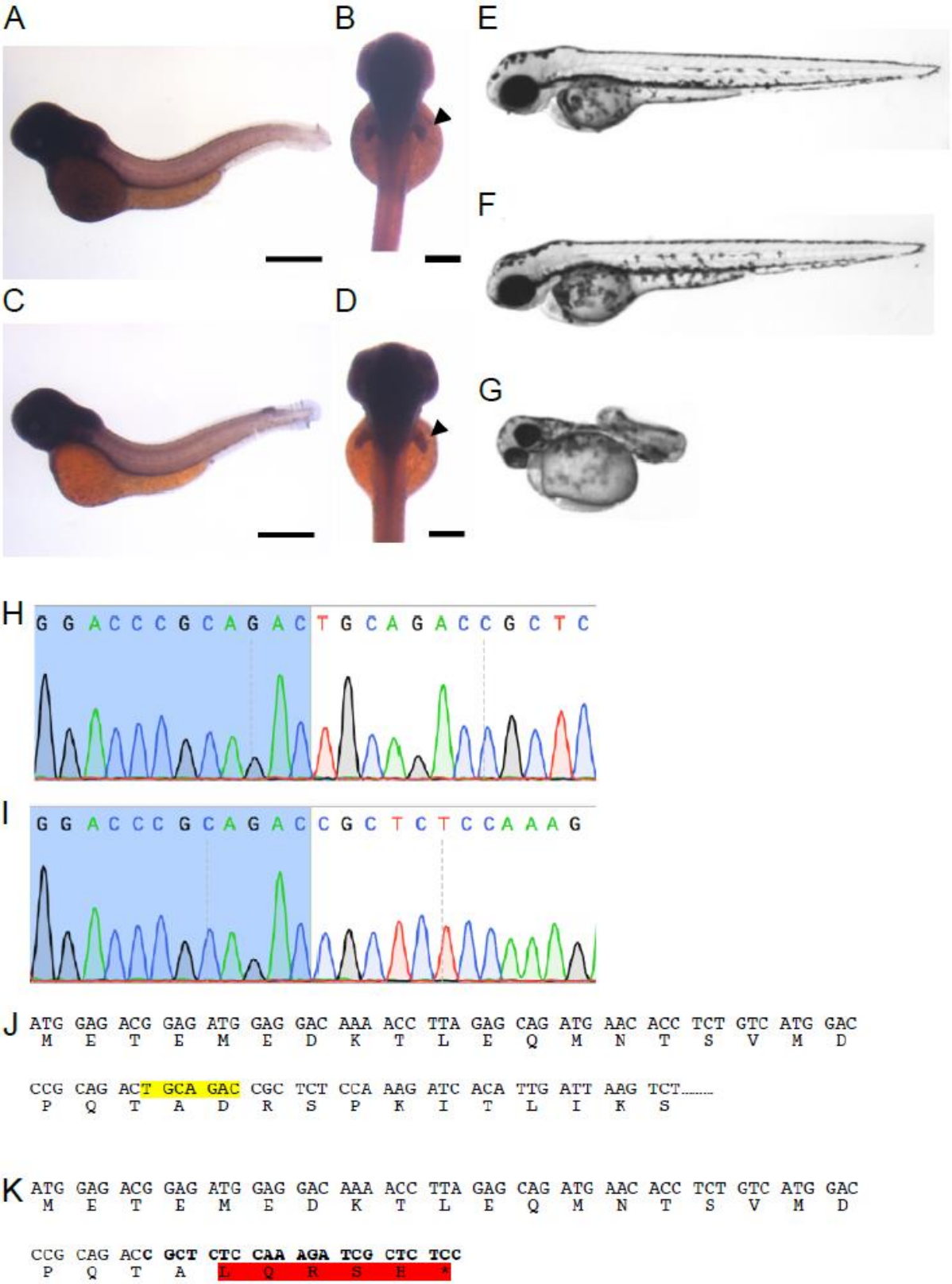

Figure S7: Zebrafish *fbxw11 in situ* hybridisation and knockdown. A-D: Whole mount *in situ* hybridisation of zebrafish *fbxw11b*. Lateral (A, C) and dorsal (B, D) views of 48 hours post fertilisation (hpf) (A, B) and 72hpf (C, D) embryos. Anterior to the left and dorsal up (A, C),

anterior to the top (B, D). Scale bars 400µm in A, C and 200µm in B, D. E-G: Lateral views (anterior to left, dorsal up) of 48hpf live wildtype zebrafish embryos injected with (E) 0.8pmol of morpholino control, (F) 0.8pmol mo^{fbxw11a} and (G) 0.8pmol mo^{fbxw11b}. H, I: Electropherograms of wildtype *fbxw11b* (H) and homozygous *fbxw11b*^{u5010} mutant (I). J, K: Wildtype (J) and *fbxw11b*^{u5010} (K) DNA and translated amino acid sequence. U5010 deletion highlighted in yellow, amino acid sequence resulting from the frameshift highlighted in red.

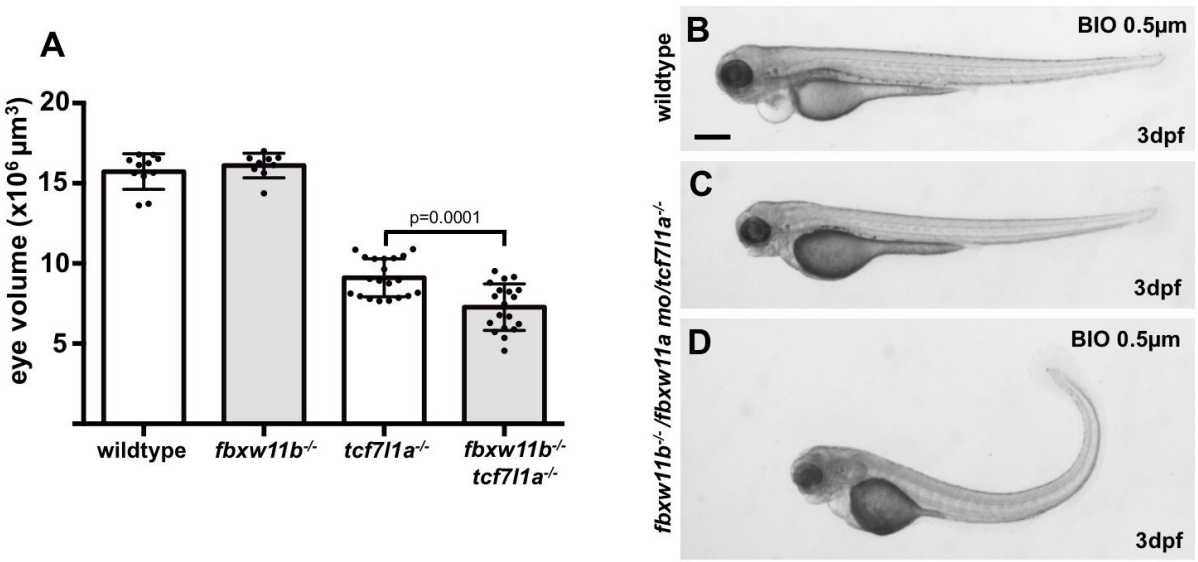

Figure S8: Zebrafish embryos with compromised *fbxw11a* and *fbxw11b* function are sensitised to enhanced Wnt/β-catenin signalling. A: Plot showing eye size in wildtype (n=11, $\tilde{x}$=1.573.007µm^3), *fbxw11b*$^{-/-}$ (n=9, $\tilde{x}$=1.611.194µm^3), *tcf7l1a*$^{-/-}$ (n=20, $\tilde{x}$=910.337µm^3) and *fbxw11b*$^{-/-}$/*tcf7l1a*$^{-/-}$ (n=19, $\tilde{x}$=727.855µm^3) embryos at 30hpf. B-D: Lateral views of 3 day post fertilisation wildtype (B) and *fbxw11b*$^{u5010/u5010}$/*fbxw11a* morphant (C, D) embryos, treated with 2% DMSO (C) or 0.5µm BIO in 2% DMSO (B, D). Scale bar=250µm.

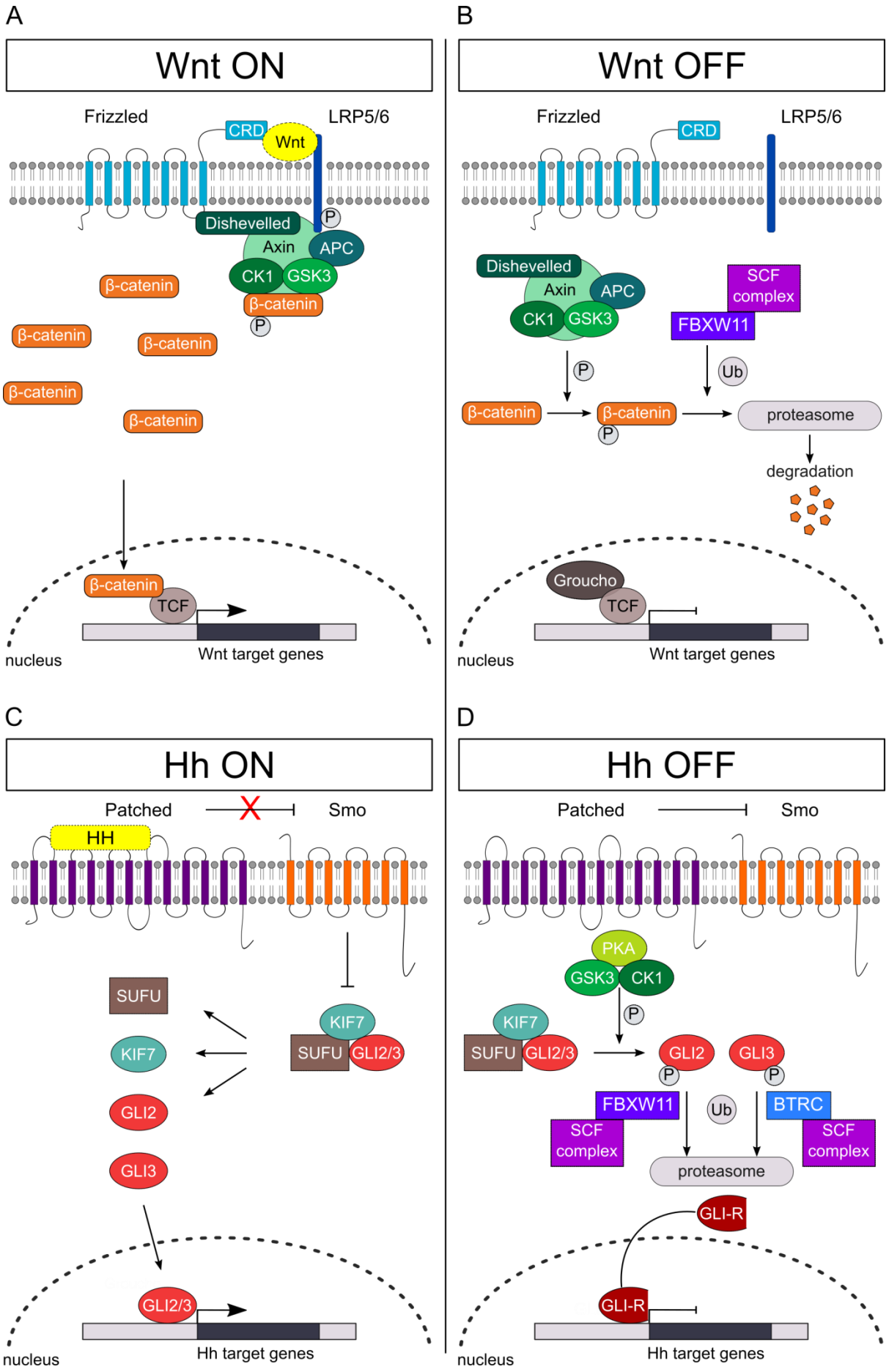
A
Wnt ON
Frizzled
LRP5/6
CRD
Wnt
Dishevelled
Axin
APC
CK1
GSK3
P
β-catenin
β-catenin
β-catenin
β-catenin
β-catenin
β-catenin
TCF
nucleus
Wnt target genes
B
Wnt OFF
Frizzled
LRP5/6
CRD
Dishevelled
Axin
APC
CK1
GSK3
SCF complex
FBXW11
P
Ub
β-catenin
β-catenin
P
proteasome
degradation
Groucho
TCF
nucleus
Wnt target genes
C
Hh ON
Patched
Smo
HH
SUFU
KIF7
GLI2
GLI3
KIF7
SUFU
GLI2/3
GLI2/3
nucleus
Hh target genes
D
Hh OFF
Patched
Smo
PKA
GSK3
CK1
P
KIF7
SUFU
GLI2/3
GLI2
GLI3
P
P
FBXW11
SCF complex
Ub
BTRC
SCF complex
proteasome
GLI-R
GLI-R
nucleus
Hh target genes

Figure S9: FBXW11 in the canonical Wnt and Hh signalling pathways. A: During Wnt signalling, extracellular Wnt ligands bind to the transmembrane Frizzled receptors and LRP5/6 co-receptors. Wnt ligand interaction with the receptor complex induces their dimerisation and the relocalisation of the "destruction complex",[2] formed by the tumour suppressor proteins Axin and APC and the serine/threonine kinases CK1α and GSK3β, to the membrane. These changes result in stabilisation and accumulation of β-catenin. Translocation of β-catenin to the nucleus and subsequent interaction with TCF transcription factors then lead to the transcriptional activation of target genes. B: In the absence of Wnt ligand, the destruction complex recruits and phosphorylates β-catenin. FBXW11 is able to recognise this phosphorylation motif and recruit the other components of the SCF (Skp1-cullin-F-box) complex, an E3 ligase complex which mediates ubiquitination and proteasomal degradation. This maintains low levels of β-catenin in the cytoplasm and the nucleus. In the nucleus, this results in the interaction of TCF transcription factors with Groucho-like transcriptional co-repressor proteins. Schematic adapted from Nusse and Clevers (2017).[3] C: In the active state, extracellular Hedgehog (HH) ligands bind to the transmembrane receptor Patched, preventing the suppression of the receptor-like protein Smoothened (Smo). This initiates a signalling cascade that results in the activation of GLI transcription factors. In particular, GLI2 and GLI3, after dissociating from the complex containing SUFU and the cilium-associated kinesin KIF7, translocate into the nucleus. As full-length proteins, they function as transcriptional activators. D: In the absence of HH signalling, Patched inhibits ciliary localisation of Smoothened, which is necessary for the activation of the pathway. In the cytoplasm, SUFU forms a complex with KIF7 and sequesters GLI2 and GLI3. Once recruited by this complex, GLI2/3 are subsequently phosphorylated by the kinases PKA, GSK3B and CK1. This promotes GLI2 and GLI3 ubiquitination, mediated by FBXW11-SCF and

BTRC-SCF complexes respectively. This directs GLI2/3 to the proteasome, where they can be either degraded or processed into truncated forms, which function as transcriptional repressors.

Supplemental Methods

Cohort description

A UK cohort of 263 individuals with ocular anomalies, principally anophthalmia, microphthalmia and coloboma (AMC), was recruited as part of a national 'Genetics of Eye and Brain anomalies' study (REC 04/Q0104/129). Informed consent was obtained according to the tenets of the Declaration of Helsinki. Additionally, 32 French individuals with developmental eye disorders were recruited via the Toulouse University Diagnostic Laboratories, France. Participant informed consent was approved by the local Ethics Committee (CPP Sud-Ouest and Outre-Mer II). Both groups had previously been screened by indication in eye development genes, but lacked a definitive genetic diagnosis. Six further individuals (2-7) were identified through GeneMatcher.[4] Clinical informed consent was obtained for Individuals 2, 3, 5 and 6 through the host institutions. Consent for Individual 4 was obtained as part of the "Genomic Study of Medical, Developmental, or Congenital Problems of Unknown Etiology" study (Pro00032301, Duke University institutional review board). Consent for Individual 7 was obtained as part of the "Ospedale Pediatrico Bambino Gesù" study (1702_OPBG_2018).

Whole exome/genome sequencing

Individual 1, UK and French AMC cases:

32 individuals with congenital eye anomalies (26 from the 263 UK cohort and 6 from the 32 French cohort) were screened by WES. WES was performed as described previously for 14/26 UK cases and 6/6 French cases.[5] WES of the remaining 12 UK cases was performed by the West Midlands Regional Genetics Laboratory (WMRGL) by Covaris shearing of sample DNA, followed by library preparation using the Agilent SureSelect Exome V6 probe kit and SureSelectXT target enrichment chemistry.

The prepared libraries were sequenced by 2 x 100bp paired-end sequencing using the Illumina HiSeq 2500 platform. Data were analysed using an in-house pipeline that consisted of the following stages: read quality assessment performed using FastQC (v0.10.1) and alignment quality using Picard's CollectHsMetrics (v1.97), followed by Samtools stats (v1.2).[6] Prior to alignment, reads were trimmed using Trimmomatic (v0.30)[7] to remove low quality bases and adapter sequences. Alignment was performed using Burrows-Wheeler Alignment tool BWA-MEM (v0.7.12-r1039)[8] against GRCh37/hg19, duplicates removed using samblaster (v0.1.21),[9] realignment performed using Abra (v0.97)[10] and qualities recalibrated using Bam utils recab (v1.0.12).[11] Variants were called using GATK HaploTypeCaller (v3.4-46) [12] according to the Broad's best practices. Variant analysis was performed using both VariantStudio v2.2 (Illumina) and a separate in-house bioinformatics pipeline. Briefly, all variants were annotated using ANNOVAR.[13] We prioritised exonic and splicing variants, excluding synonymous variants. Within ANNOVAR, alternate allele frequencies were annotated for each variant using several public databases, including the 1000 Genomes Project (version August 2015),[14] the Exome Aggregation Consortium Browser (ExAC, v0.3)

and gnomAD (version 2017).[15] A minor allele frequency (MAF) threshold of ≤1% was chosen for homozygous variants and ≤0.1% for heterozygous variants. Various prediction scores for the impact on function were annotated using dbNSFP v3.3a.[16; 17] Prediction algorithms, such as the Combined Annotation Dependent Depletion (CADD[18]) and the meta-predictors MetaSVM and MetaLR[19] were used to interpret the potential pathogenicity of nonsynonymous variants. When parental data was available, trio analysis was performed to identify *de novo* variants.

Individual 2:

For Individual 2, genomic DNA extraction, exome library preparation, sequencing, bioinformatics pipeline, and data analyses were performed at Ambry Genetics (Aliso Viejo, CA) on the proband and their parents as previously described.[20; 21] Briefly, samples were prepared and sequenced using paired-end, 100 cycle chemistry on the Illumina HiSeq 2500 sequencer. Exome enrichment was performed using the SeqCap EZ VCRome 2.0 (Roche NimblGen). Variants were confirmed by Sanger sequencing.

Individual 3:

For Individual 3 diagnostic WES was performed for the proband and their parents in a clinical laboratory. Exomes were enriched using the SureSelect XT Human All Exon V5 kit (Agilent) and sequenced in rapid run mode on the HiSeq 2500 sequencing system (Illumina) at a mean target depth of 100x. The target was defined as all coding exons of UCSC and Ensembl +/- 20bp intron flanks. At this depth ~95% of the target was covered at least 15x. Reads were aligned to hg19 using BWA (BWA-MEM v0.7.5a) and variants were called using the GATK haplotype caller (v2.7-2). Detected variants were annotated, filtered and

prioritised using the Bench NGS Lab platform (Cartagenia, Leuven, Belgium). A trio analysis of the proband and both parents was performed. Analysis was based upon a tiered analysis approach. The first tier analysed genes in which variants are known to contribute to intellectual disability. The second tier filtered for *de novo* variants and the last tier filtered for recessive variants. Variant confirmation and segregation analyses were performed using standard Sanger sequencing (primer sequences available upon request).

Individual 4:

Whole exome trio screening for Individual 4 was performed as described previously.[22]

Individual 5:

For Individual 5 a trio-based WES approach was undertaken. DNA from patient and parents was subjected to exome capture using NimbleGen SeqCap EZ MedExome (Roche), followed by sequencing on an Illumina NextSeq550 to a mean coverage of 118x, with 95% of targeted bases covered with minimum 20x coverage. Raw reads were aligned using the Burrows-Wheeler Alignment tool (BWA-MEM) v0.7.15[23] and the GATK Best Practice pipeline v3.8–0 was used for variant calling.[12] Annotation and filtering of variants were performed using VarSeq 2.0.2 (Golden Helix).

Individual 6:

Genomic DNA for Individual 6 was enriched for the complete coding regions and splice site junctions using a proprietary capture system for next-generation sequencing with CNV calling (NGS-CNV) (GeneDx). Enriched targets were sequenced with paired-end reads on an Illumina platform and reads assembled and aligned to NCBI RefSeq transcripts and human

genome build GRCh37/hg19. Using a custom-developed analysis tool (XomeAnalyzer), data were filtered and analysed to identify sequence variants and most deletions and duplications involving three or more coding exons.[24] Reported clinically significant variants were confirmed by an appropriate orthogonal method.

Individual 7:

For Individual 7, sequencing was performed using Illumina HiSeq X and the resulting 150bp paired-end reads were aligned to the GRCh38 reference genome using bwa mem (v0.7.12).[8] Data analysis was performed using an in-house implemented pipeline, mainly based on the Genome Analysis Toolkit (GATK v3.7)[25] framework, as previously reported.[26-28] GATK/Picard tools (v3.7/2.3) were used for removing duplicates, base quality recalibration and variant calling. SNVs and small INDELs were identified by means of the GATK's HaplotypeCaller tool used in gVCF mode, followed by family-level joint genotyping and phasing; finally, variants were quality-filtered using a VQSR strategy, according to GATK's 2016 best practices.[12] Following the exclusion of any relevant structural variants, by means of Delly2,[29] we annotated and prioritised SNV/INDELs with functional effect on coding sequences and splicing. To retain private and clinically associated variants, we removed common SNPs (dbSNP151, MAF >1%), selecting annotated variants with unknown frequency or having minor allele frequency (MAF) <0.1% (gnomAD v2.0), and occurring with a frequency <1% in an in-house database including frequency data from approximately 1300 population-matched WES. To analyse variants in the CDS and splice regions (variants located from −3 to +8 with respect to an exon-intron junction) we took advantage of the pipeline we previously developed for WES data,[27; 28] using SnpEff toolbox (v4.3) and dbNSFP (v3.5).[19; 30; 31] The

functional impact of variants was analysed by CADD v1.4 and InterVar v2.0 algorithms,[18; 32] to obtain clinical interpretation according to ACMG/AMP 2015 guidelines.[32]

Targeted gene sequencing

Targeted resequencing of 187 genes, including *FBXW11*, was performed for the 26/32 French individuals with undiagnosed microphthalmia or anophthalmia, as described previously.[5]

Candidate gene screening of FBXW11

Single gene screening for variants in the exons and a minimum of 50bp of flanking intronic sequence of *FBXW11* was performed by either high-resolution melt analysis[33] or direct Sanger sequencing. All potential variants identified using high-resolution melt analysis were validated by Sanger sequencing. Primers and amplification conditions are available upon request.

The locations of all variants identified in this study are given according to the human genome assembly GRCh37/hg19, gene accession number NM_012300.2 and protein ID NP_036432.2.

Array Comparative Genome Hybridisation (aCGH) of AMC cohort cases

Array CGH data were available for 77 of the 263 UK individuals with AMC. Fifty-seven patients, including Individual 1, were analysed by aCGH using the Agilent (USA) 44K oligonucleotide platform (design 017457), which included six probes located within *FBXW11*. Twenty additional patients received aCGH using standard UK National Health

Service (NHS)-validated diagnostic techniques, of which 10 were run on a customised array including *FBXW11*, with exon-level density of probes.

Bioinformatic variant modelling

PolyPhen-2,[34] SIFT,[35] CADD[36] and InterVar[32] software tools were used to predict the functional effects of missense variants. For each variant, GERP++ rejection scores (RS)[37] are also indicated (Table S1), as position-specific estimates of mammalian conservation. Positive RS represent a substitution deficit, which suggests that a site may be under evolutionary constraint.

The distribution of constrained coding regions (CCRs) across *FBXW11* was also analysed, according to the model developed by Havrilla *et al.*[1] CCRs with the highest percentiles are the most constrained coding regions across the human genome. Ranking percentiles of the three CCRs harbouring the variants discussed in this study are indicated in Table S1.

Protein structures were obtained from the Research Collaboratory for Structural Bioinformatics Protein Data Bank (RCSB PDB)[38] and visualised using PyMOL (The PyMOL Molecular Graphics System, Version 2.0 Schrödinger, LLC). Pairwise alignments of protein sequences were performed using EMBOSS Needle.[39] Homology modelling of the human FBXW11 (NP_036432.2, residues 110-518) was based on the crystal structure of the human BTRC (Protein Data Bank, PDB, 1P22, chain A) employing the pairwise sequence alignment. Skp1 and β-catenin molecules co-crystallized with BTRC in the PDB structure 1P22 were added in same relative binding poses to the FBXW11 model making side chain optimisation of the resulting FBXW11/Skp1/β-catenin complex. Homology modelling and side chain

optimisation were performed employing same procedure as previously described.[40] To show potentially alternative binding modes of peptides to the WD40 domain of FBXW11, we searched peptide ligands bound to WD40 domain-containing proteins in the PDB database and found the following complexes: cyclinE C-terminal degron bound to FBXW7 (PDB 2OVQ); cyclinE N-terminal degron bound to FBXW7 (PDB 2OVR); DISC1 bound to FBXW7 (PDB 5V4B); high-affinity CPD phosphopeptide from human cyclin E bound to Cdc4 (PDB 1NEX); SIC1 bound to Cdc4 (PDB 3V7D). The structures of these peptides were placed onto the WD40 domain of FBXW11 employing the same binding poses relative to the WD40 proteins present in the parent PDB structures. Mutational modelling of variants was performed using the FoldX plugin[41] within the YASARA program. The mean ΔΔG (difference in energy between wildtype and variant) was calculated for five replicate runs.

In situ hybridisation

Nonradioactive RNA *in situ* hybridisation was performed on human formalin fixed, paraffin embedded embryo sections from Carnegie Stages (CS) 15-21, as described elsewhere.[42] Human embryos were obtained from the MRC/Wellcome Trust Human Developmental Biology Resource, UCL, with full ethical approval. Two probes were generated using the primers CTTCAGGTCTGCACGTCCTAC and GCTATCGCACCCACTCTAGC, amplifying a unique 233bp region of the *FBXW11* 5' UTR, and AATGTCCAGGGCTTTCATTT and TGACTCCAGCAACTTTGAGG, amplifying a 375bp region of the 3' UTR. Both probes were designed to target all three *FBXW11* human isoforms (NM_012300, NM_033644, and NM_033645). Probes for the chondrogenic marker *SOX9* were synthesised as described by Morais da Silva *et al*.[43]

Zebrafish husbandry and mutant allele

Adult zebrafish were kept under standard husbandry conditions and embryos obtained by natural spawning. Ethical approval for zebrafish experiments was obtained from the Home Office UK according to the Animal Scientific Procedures Act 1986. Wildtype and *tcf7l1a*^{m88144} mutant embryos were raised at 28^{o}C and staged according to Kimmel *et al*. [45]

Zebrafish morpholino microinjection

Zebrafish embryos were co-injected with 10nl of a mix of 50pg of GFP mRNA and morpholinos at the indicated amount at 1-cell stage. Only embryos with an even GFP fluorescent expression at 1 day post fertilisation were analysed.

Generation of CRISPR fbxw11b mutants

CRISPR/Cas9 mutations were induced in the second exon of *fbxw11b*, which codes for the start of the open reading frame, by co-injecting 150pg of Cas9 mRNA and 30pg guide RNA (gRNA) to a 10nl volume into the yolk of one-cell stage zebrafish embryos. The gRNA, designed to anneal the target GGAGAGCGGTCTGCAGTCTG, was transcribed with a HiScribe T7 High Yield RNA Synthesis Kit (New England Biolabs) followed by DNase I digestion (New England Biolabs), and purified with the RNeasy MiniKit (Qiagen). Capped Cas9 mRNA was transcribed from an *XbaI*-digested pT3TS-nCas9n (Addgene) plasmid, using the mMessage mMachine T3 Transcription Kit (Life Technologies) followed by polyadenylation with the Poly(A) Tailing Kit (Life Technologies). The mRNA was purified using the RNeasy MiniKit (Qiagen). We tested the efficacy of mutation induction by melting curve analysis of amplicons generated with primers F (CGTCTGCAGAACACCTCTGT) and R (TCAAACCTGAGGCACCACTC) and using genomic DNA from fin clips or embryos as a

template. Genomic DNA was isolated by HotSHOT method and *fbxw11*^{U5010} mutations were genotyped by KASP assays (K Biosciences).

Zebrafish in situ hybridisation, plastic sections, alcian blue staining, eye size measurement and BIO treatment

Zebrafish embryos were fixed in 4% paraformaldehyde for an hour at room temperature, then dehydrated and kept in methanol. *In situ* hybridisation was performed according to Thisse and Thisse,[46] except that embryos were left in NBT/BCIP staining for three days at room temperature changing the substrate daily.

For plastic sections, embryos were embedded in resin using the JB-4 kit (Sigma). Embryos were step dehydrated into methanol, then incubated in 50% JB-4 kit SolutionA/methanol for 1 hour, then transferred to 100% SolutionA for overnight incubation at 4^{o}C. Embryos were then placed in rubber mounting moulds, the excess SolutionA was removed and replaced with a 24:1 mix of room temperature pre-warmed active SolutionA and SolutionB. After orienting the embryos, the mould was placed in a hermetic chamber together with a small pot of liquid nitrogen to promote polymerisation of the resin. The chamber was sealed once the liquid nitrogen was evaporated and kept overnight at room temperature. The resin blocks were glued to acrylic supports using Technovit 3040 Kit (Kulzer) and sectioned with a Leica Jung RM2055 micrometer at 8µm. Each plastic section was placed on a 30µl drop of water on a glass slide and manually unfolded under a dissecting microscope using forceps. Glass slides were then placed on a heat plate at 37^{o}C until the water had evaporated. Sections were then covered with a 4µg/ml DAPI solution for 20 minutes, washed 3 times in water for 10 minutes each and covered with DPX mountant (Sigma) and a coverslip.

For alcian blue staining, fixed embryos were dehydrated in 70% ethanol/PBS for 5 minutes and then incubated over night at room temperature in a staining solution of 0.02% alcian blue, 0.2M $MgCl_2$ and 60% Ethanol in water. The staining solution was washed off in PBS and embryos were imaged under a dissecting microscope.

The eye size of 30hpf embryos was assessed as previously described.[47] BIO (Sigma, B1686) was diluted to 0.5µm in 2% DMSO in embryo medium and embryos were incubated in this solution from 24hpf until 3 days post fertilisation.

Supplemental References

1. Havrilla, J.M., Pedersen, B.S., Layer, R.M., and Quinlan, A.R. (2019). A map of constrained coding regions in the human genome. Nat Genet 51, 88-95.
2. Stamos, J.L., and Weis, W.I. (2013). The beta-catenin destruction complex. Cold Spring Harb Perspect Biol 5, a007898.
3. Nusse, R., and Clevers, H. (2017). Wnt/beta-Catenin Signaling, Disease, and Emerging Therapeutic Modalities. Cell 169, 985-999.
4. Sobreira, N., Schiettecatte, F., Valle, D., and Hamosh, A. (2015). GeneMatcher: a matching tool for connecting investigators with an interest in the same gene. Hum Mutat 36, 928-930.
5. Ragge, N., Isidor, B., Bitoun, P., Odent, S., Giurgea, I., Cogne, B., Deb, W., Vincent, M., Le Gall, J., Morton, J., et al. (2018). Expanding the phenotype of the X-linked BCOR microphthalmia syndromes. Hum Genet.
6. Li, H., Handsaker, B., Wysoker, A., Fennell, T., Ruan, J., Homer, N., Marth, G., Abecasis, G., Durbin, R., and Genome Project Data Processing, S. (2009). The Sequence Alignment/Map format and SAMtools. Bioinformatics 25, 2078-2079.
7. Bolger, A.M., Lohse, M., and Usadel, B. (2014). Trimmomatic: a flexible trimmer for Illumina sequence data. Bioinformatics 30, 2114-2120.
8. Li, H., and Durbin, R. (2010). Fast and accurate long-read alignment with Burrows-Wheeler transform. Bioinformatics 26, 589-595.
9. Faust, G.G., and Hall, I.M. (2014). SAMBLASTER: fast duplicate marking and structural variant read extraction. Bioinformatics 30, 2503-2505.
10. Mose, L.E., Wilkerson, M.D., Hayes, D.N., Perou, C.M., and Parker, J.S. (2014). ABRA: improved coding indel detection via assembly-based realignment. Bioinformatics 30, 2813-2815.
11. Jun, G., Wing, M.K., Abecasis, G.R., and Kang, H.M. (2015). An efficient and scalable analysis framework for variant extraction and refinement from population-scale DNA sequence data. Genome Res 25, 918-925.

12. Van der Auwera, G.A., Carneiro, M.O., Hartl, C., Poplin, R., Del Angel, G., Levy-Moonshine, A., Jordan, T., Shakir, K., Roazen, D., Thibault, J., et al. (2013). From FastQ data to high confidence variant calls: the Genome Analysis Toolkit best practices pipeline. Curr Protoc Bioinformatics 43, 11 10 11-33.
13. Wang, K., Li, M., and Hakonarson, H. (2010). ANNOVAR: functional annotation of genetic variants from high-throughput sequencing data. Nucleic Acids Res 38, e164.
14. Consortium, G.P., Auton, A., Brooks, L.D., Durbin, R.M., Garrison, E.P., Kang, H.M., Korbel, J.O., Marchini, J.L., McCarthy, S., McVean, G.A., et al. (2015). A global reference for human genetic variation. Nature 526, 68-74.
15. Lek, M., Karczewski, K.J., Minikel, E.V., Samocha, K.E., Banks, E., Fennell, T., O'Donnell-Luria, A.H., Ware, J.S., Hill, A.J., Cummings, B.B., et al. (2016). Analysis of protein-coding genetic variation in 60,706 humans. Nature 536, 285-291.
16. Liu, X., Jian, X., and Boerwinkle, E. (2011). dbNSFP: a lightweight database of human nonsynonymous SNPs and their functional predictions. Hum Mutat 32, 894-899.
17. Liu, X., Wu, C., Li, C., and Boerwinkle, E. (2016). dbNSFP v3.0: A One-Stop Database of Functional Predictions and Annotations for Human Nonsynonymous and Splice-Site SNVs. Hum Mutat 37, 235-241.
18. Kircher, M., Witten, D.M., Jain, P., O'Roak, B.J., Cooper, G.M., and Shendure, J. (2014). A general framework for estimating the relative pathogenicity of human genetic variants. Nat Genet 46, 310-315.
19. Dong, C., Wei, P., Jian, X., Gibbs, R., Boerwinkle, E., Wang, K., and Liu, X. (2015). Comparison and integration of deleteriousness prediction methods for nonsynonymous SNVs in whole exome sequencing studies. Hum Mol Genet 24, 2125-2137.
20. Farwell, K.D., Shahmirzadi, L., El-Khechen, D., Powis, Z., Chao, E.C., Tippin Davis, B., Baxter, R.M., Zeng, W., Mroske, C., Parra, M.C., et al. (2015). Enhanced utility of family-centered diagnostic exome sequencing with inheritance model-based analysis: results from 500 unselected families with undiagnosed genetic conditions. Genet Med 17, 578-586.
21. Smith, E.D., Radtke, K., Rossi, M., Shinde, D.N., Darabi, S., El-Khechen, D., Powis, Z., Helbig, K., Waller, K., Grange, D.K., et al. (2017). Classification of Genes: Standardized Clinical Validity Assessment of Gene-Disease Associations Aids Diagnostic Exome Analysis and Reclassifications. Hum Mutat 38, 600-608.
22. Zhu, X., Petrovski, S., Xie, P., Ruzzo, E.K., Lu, Y.F., McSweeney, K.M., Ben-Zeev, B., Nissenkorn, A., Anikster, Y., Oz-Levi, D., et al. (2015). Whole-exome sequencing in undiagnosed genetic diseases: interpreting 119 trios. Genet Med 17, 774-781.
23. Li, H. (2014). Aligning sequence reads, clone sequences and assembly contains with BWA-MEM. arXiv.org.
24. Retterer, K., Scuffins, J., Schmidt, D., Lewis, R., Pineda-Alvarez, D., Stafford, A., Schmidt, L., Warren, S., Gibellini, F., Kondakova, A., et al. (2015). Assessing copy number from exome sequencing and exome array CGH based on CNV spectrum in a large clinical cohort. Genet Med 17, 623-629.
25. McKenna, A., Hanna, M., Banks, E., Sivachenko, A., Cibulskis, K., Kernytsky, A., Garimella, K., Altshuler, D., Gabriel, S., Daly, M., et al. (2010). The Genome Analysis Toolkit: a MapReduce framework for analyzing next-generation DNA sequencing data. Genome Res 20, 1297-1303.

26. Linderman, M.D., Brandt, T., Edelmann, L., Jabado, O., Kasai, Y., Kornreich, R., Mahajan, M., Shah, H., Kasarskis, A., and Schadt, E.E. (2014). Analytical validation of whole exome and whole genome sequencing for clinical applications. BMC Med Genomics 7, 20.
27. Sferra, A., Baillat, G., Rizza, T., Barresi, S., Flex, E., Tasca, G., D'Amico, A., Bellacchio, E., Ciolfi, A., Caputo, V., et al. (2016). TBCE Mutations Cause Early-Onset Progressive Encephalopathy with Distal Spinal Muscular Atrophy. Am J Hum Genet 99, 974-983.
28. Bauer, C.K., Calligari, P., Radio, F.C., Caputo, V., Dentici, M.L., Falah, N., High, F., Pantaleoni, F., Barresi, S., Ciolfi, A., et al. (2018). Mutations in KCNK4 that Affect Gating Cause a Recognizable Neurodevelopmental Syndrome. Am J Hum Genet 103, 621-630.
29. Rausch, T., Zichner, T., Schlattl, A., Stutz, A.M., Benes, V., and Korbel, J.O. (2012). DELLY: structural variant discovery by integrated paired-end and split-read analysis. Bioinformatics 28, i333-i339.
30. Cingolani, P., Platts, A., Wang le, L., Coon, M., Nguyen, T., Wang, L., Land, S.J., Lu, X., and Ruden, D.M. (2012). A program for annotating and predicting the effects of single nucleotide polymorphisms, SnpEff: SNPs in the genome of Drosophila melanogaster strain w1118; iso-2; iso-3. Fly (Austin) 6, 80-92.
31. Liu, X., Jian, X., and Boerwinkle, E. (2013). dbNSFP v2.0: a database of human non-synonymous SNVs and their functional predictions and annotations. Hum Mutat 34, E2393-2402.
32. Li, Q., and Wang, K. (2017). InterVar: Clinical Interpretation of Genetic Variants by the 2015 ACMG-AMP Guidelines. Am J Hum Genet 100, 267-280.
33. Kennerson, M.L., Warburton, T., Nelis, E., Brewer, M., Polly, P., De Jonghe, P., Timmerman, V., and Nicholson, G.A. (2007). Mutation scanning the GJB1 gene with high-resolution melting analysis: implications for mutation scanning of genes for Charcot-Marie-Tooth disease. Clin Chem 53, 349-352.
34. Adzhubei, I.A., Schmidt, S., Peshkin, L., Ramensky, V.E., Gerasimova, A., Bork, P., Kondrashov, A.S., and Sunyaev, S.R. (2010). A method and server for predicting damaging missense mutations. Nat Methods 7, 248-249.
35. Ng, P.C., and Henikoff, S. (2003). SIFT: Predicting amino acid changes that affect protein function. Nucleic Acids Res 31, 3812-3814.
36. Rentzsch, P., Witten, D., Cooper, G.M., Shendure, J., and Kircher, M. (2019). CADD: predicting the deleteriousness of variants throughout the human genome. Nucleic Acids Res 47, D886-D894.
37. Davydov, E.V., Goode, D.L., Sirota, M., Cooper, G.M., Sidow, A., and Batzoglou, S. (2010). Identifying a high fraction of the human genome to be under selective constraint using GERP++. PLoS Comput Biol 6, e1001025.
38. Berman, H.M., Westbrook, J., Feng, Z., Gilliland, G., Bhat, T.N., Weissig, H., Shindyalov, I.N., and Bourne, P.E. (2000). The Protein Data Bank. Nucleic Acids Res 28, 235-242.
39. Needleman, S.B., and Wunsch, C.D. (1970). A general method applicable to the search for similarities in the amino acid sequence of two proteins. J Mol Biol 48, 443-453.
40. Motta, M., Fidan, M., Bellacchio, E., Pantaleoni, F., Schneider-Heieck, K., Coppola, S., Borck, G., Salviati, L., Zenker, M., Cirstea, I.C., et al. (2018). Dominant Noonan syndrome-causing LZTR1 mutations specifically affect the kelch domain substrate-recognition surface and enhance RAS-MAPK signaling. Hum Mol Genet.

41. Schymkowitz, J., Borg, J., Stricher, F., Nys, R., Rousseau, F., and Serrano, L. (2005). The FoldX web server: an online force field. Nucleic Acids Res 33, W382-388.
42. Lai, C.S., Gerrelli, D., Monaco, A.P., Fisher, S.E., and Copp, A.J. (2003). FOXP2 expression during brain development coincides with adult sites of pathology in a severe speech and language disorder. Brain 126, 2455-2462.
43. Morais da Silva, S., Hacker, A., Harley, V., Goodfellow, P., Swain, A., and Lovell-Badge, R. (1996). Sox9 expression during gonadal development implies a conserved role for the gene in testis differentiation in mammals and birds. Nat Genet 14, 62-68.
44. Kim, C.H., Oda, T., Itoh, M., Jiang, D., Artinger, K.B., Chandrasekharappa, S.C., Driever, W., and Chitnis, A.B. (2000). Repressor activity of Headless/Tcf3 is essential for vertebrate head formation. Nature 407, 913-916.
45. Kimmel, C.B., Ballard, W.W., Kimmel, S.R., Ullmann, B., and Schilling, T.F. (1995). Stages of embryonic development of the zebrafish. Dev Dyn 203, 253-310.
46. Thisse, C., and Thisse, B. (2008). High-resolution in situ hybridization to whole-mount zebrafish embryos. Nat Protoc 3, 59-69.
47. Young, R.M., Hawkins, T.A., Cavodeassi, F., Stickney, H.L., Schwarz, Q., Lawrence, L.M., Wierzbicki, C., Cheng, B.Y., Luo, J., Ambrosio, E.M., et al. (2019). Compensatory growth renders Tcf7l1a dispensable for eye formation despite its requirement in eye field specification. eLife 8.